UNIVERSIDADE DE LISBOA
FACULDADE DE CIÊNCIAS
DEPARTAMENTO DE FÍSICA

Engineering Tissue with Acoustic Manipulation

Camila Filipa Querido Canhoto

Mestrado em Engenharia Biomédica e Biofísica

Dissertação orientada por:
Oscar O'Dwyer Lancaster-Jones
Nuno Matela

2025

Acknowledgements

I would like to thank Dr. Daniela Duarte Campos and all the members of Duarte Campos Lab (ZMBH) for welcoming me in their group and for always being available to help me overcome both professional and personal challenges. My gratitude goes especially to my supervisor, Dr. Oscar O'Dwyer Lancaster-Jones, for teaching me most of the concepts regarding acoustic manipulation, for all the guidance throughout the development of this dissertation, and for always encouraging me with his positivity.

Thank you, Prof. Dr. Nuno Matela, for your support and availability. I am truly grateful to be your student.

I would like to express my deepest appreciation to my family, especially my mother, who never stopped believing in me and who has always been my greatest supporter. Everything I have achieved in life, I owe it to you. Thank you, father, for your encouragement and for providing the right conditions for me to learn and become an engineer. I would not be writing this dissertation without having you both by my side.

I also want to acknowledge my boyfriend for being my motivation and for inspiring me to be a better person every day. Pedro, thank you for all the love and support, you make life so much softer.

Thank you to all my friends who were part of my academic journey. A special thanks goes to Bárbara, Mafalda, Solange, Raquel and Sara, for all the laughs and tears, and for never letting me quit. You were a key part of my life during these five years.

Finally, I want to thank the Erasmus+ Programme for helping me achieve my goals by funding my internship in Heidelberg.

Resumo

A escassez de órgãos disponíveis para transplante é um problema cada vez mais urgente na atualidade, com o número de pessoas necessitadas a aumentar exponencialmente. A engenharia de tecidos é uma área de investigação que procura solucionar esta questão, através do desenvolvimento que técnicas que permitem regenerar, reparar ou substituir tecidos danificados. Além de dar resposta à oferta limitada de órgãos, a engenharia de tecidos permite a criação de modelos tridimensionais (3D), importantes no estudo e investigação de patologias e desenvolvimento de fármacos.

A engenharia de tecidos baseia-se essencialmente em três componentes: células, um suporte estrutural (*scaffolds*) e um ambiente propício ao seu desenvolvimento. É importante imitar as condições existentes num tecido biológico natural para permitir o crescimento e a proliferação das células, pelo que o *scaffold* escolhido deve imitar eficazmente a matriz extracelular (ECM, do inglês *Extracellular Matrix)* do tecido pretendido. No entanto, os *scaffolds* têm falta de propriedades condutivas e arquiteturas fibrosas, que são características importantes de certas ECMs, como a ECM cardíaca. Assim, outras alternativas têm sido estudadas. Os esferoides, agregados 3D de células, surgem como uma solução para este problema, dado que imitam funções celulares de forma mais eficaz.

Certos tecidos como os tecidos anisotrópicos, por exemplo tecidos nervosos e cardíacos, possuem uma organização celular específica, essencial para garantir a funcionalidade dos mesmos. Assim, na engenharia de tecidos, é importante existir este controlo na organização celular de tecidos fabricados *ex vivo*.

Existem diferentes métodos que permitem alinhar e padronizar células. Técnicas baseadas em fluxos de fluidos controlados, *bioprinting* e estratégias como a utilização de substratos microestruturados são alguns dos métodos utilizados no alinhamento de células, mas apresentam várias limitações como incapacidade em controlar espacialmente com precisão estruturas 3D. A manipulação acústica é uma técnica que se destaca destes métodos por oferecer uma estratégia não invasiva, sem recurso a marcadores externos e com elevada resolução. Este método consiste na utilização de ondas acústicas estacionárias, que possuem zonas de alta e baixa pressão, denominadas por antinodos e nodos, respetivamente. Perante uma onda acústica estacionária, partículas com um diâmetro inferior a metade do comprimento de onda tendem a fixar-se nas zonas onde a pressão é mínima, isto é, nos nodos. Assim, é possível criar padrões de partículas ou células por manipulação acústica.

As ondas acústicas estacionárias são criadas através da sobreposição de duas ondas sonoras, com a mesma frequência e amplitude, que se propagam na mesma direção em sentidos opostos. Isto pode acontecer quer por reflexão, quer por emissão de duas ondas idênticas. Existem dois tipos de ondas sonoras utilizadas nesta área da engenharia de tecidos: as *Surface Acoustic Waves* (SAWs) e as *Bulk Acoustic Waves* (BAWs). As primeiras propagam-se ao longo da superfície de um material e são geradas por transdutores interdigitais (IDTs), ao passo que as segundas se propagam pelo interior do material, sendo formadas por transdutores de titanato zirconato de chumbo (PZT).

Existem diversos fatores que influenciam a propagação das ondas sonoras, incluindo a frequência, a voltagem inicial e a impedância acústica do meio de propagação, por exemplo. A presente dissertação apresenta uma breve revisão literária dos sistemas de manipulação acústica desenvolvidos por diferentes grupos de investigação, onde são destacadas as diferenças entre cada um e as informações cientificamente relevantes que foram concluídas após experiências realizadas com os mesmos. Foram

também descritos os diferentes fatores provados por estes grupos de investigação como sendo influentes no campo acústico e no alinhamento de células.

O objetivo do presente trabalho consistiu em compreender experiencialmente a influência de vários parâmetros no alinhamento de esferoides de Fibroblastos Dérmicos Humanos (HDF, do inglês *Human Dermal Fibroblasts*) e desenvolver um *setup* otimizado para este propósito, baseado na tecnologia BAWs. Para tal, foi utilizada a metodologia *Six-Sigma*: *Define-Measure-Analyse-Design-Validate*.

Inicialmente, foram estabelecidos os requisitos do cliente, isto é, dos investigadores, através de conversas e de experiências preliminares conduzidas com *setups* existentes no laboratório onde este trabalho foi desenvolvido (Duarte Campos Lab, ZMBH). Posteriormente, estes requisitos foram convertidos em parâmetros mensuráveis, e uma análise aprofundada dos diferentes fatores que influenciam a propagação de ultrassons foi realizada experimentalmente. Esta análise teve por base o estudo do movimento de micropartículas e esferoides HDF, através da captura de imagens num microscópio. No caso das micropartículas, foi avaliado o tempo até estas estarem alinhadas, através de ferramentas como o *ImageJ*, que permitiu a realização de uma Tesselação de *Voronoï*. Através de um *script Python*, foi determinada a distorção da onda com base na raíz do desvio quadrático médio (RMSD, do inglês *Root Mean Square Deviation*) dos centros de massa. Já no caso dos esferoides, foi possível analisar o seu deslocamento e velocidade média, através de um *script MATLAB* que realizava o rastreamento dos mesmos ao longo do tempo. Além destas análises, foram também realizadas medições de amplitude, que funcionaram como um método de avaliação da perda de energia da onda após propagação.

As experiências conduzidas permitiram concluir o efeito que diversos fatores têm no campo acústico e consequentemente no alinhamento dos esferoides. Percebeu-se que a distância entre os transdutores tem um grande impacto nos valores de amplitude medidos, assim como o volume de água utilizado para propagação da onda sonora, e a presença de descontinuidades extra, como uma *chamber slide* para deposição dos esferoides em ambiente estéril. Além disso, foram estabelecidas comparações entre *setups* existentes, e foram realizados testes estatísticos para concluir qual deles permite uma melhor propagação das ondas sonoras. Não foi detetada nenhuma diferença estatisticamente relevante entre *setups*. No entanto, foi evidenciada uma tendência de um *setup* em específico, que foi considerada como tendo relevância prática e como sendo uma observação útil para a orientação de experiências subsequentes. Adicionalmente, percebeu-se que a frequência do sinal tem um impacto significativo na amplitude da onda após a sua propagação.

Todas as experiências conduzidas permitiram o posterior desenvolvimento da *House of Quality* e de soluções de *design*, que foram avaliadas tendo em conta as suas características. As melhores alternativas foram analisadas em estudos piloto, tendo sido possível determinar qual a solução com a melhor *performance*. Contudo, não foi realizada uma validação desta alternativa no âmbito deste trabalho, dado que experiências e análises complementares eram necessárias para aumentar a reprodutibilidade e, consequentemente, a confiabilidade dos resultados.

Foram encontradas algumas limitações nos métodos de avaliação do movimento das partículas e dos esferoides. A escolha da região da captura das imagens influenciava potencialmente os resultados, dado que a distribuição e o movimento, tanto das partículas como dos esferoides, não eram homogéneos na câmara onde estavam inseridos. Adicionalmente, percebeu-se que o *script* desenvolvido no *ImageJ* nem sempre detetava com alta exatidão a posição de todas as partículas, o que também influenciou negativamente os resultados obtidos. Além disso, no âmbito deste trabalho, não foi possível adaptar esse *script* para a análise do movimento dos esferoides, devido a diferenças de tamanho entre as partículas e

estas estruturas. Assim, foram apenas avaliados o deslocamento médio e a velocidade média dos esferoides através de um código MATLAB, tendo o alinhamento dos mesmos sido avaliado somente qualitativamente por visualização direta dos resultados.

Apesar de não ter sido possível desenvolver um *setup* que estivesse perfeitamente otimizado e validado para a manipulação acústica de esferoides HDF, os restantes objetivos do presente trabalho foram cumpridos. Os diferentes fatores que influenciam o alinhamento destas estruturas celulares foram estudados e diversas condições que permitem ressonância e, consequentemente melhores resultados, foram determinadas. Este trabalho permitiu desta forma uma melhor compreensão da engenharia de tecidos com manipulação acústica, sendo importante a sua consideração em trabalhos futuros relacionados com o tema.

Palavras-chave: Manipulação Acústica, Engenharia de Tecidos, Alinhamento, Amplitude, Propagação de ondas.

Abstract

Tissue engineering is an emerging technology that addresses the limitations of organ transplantation by providing strategies to regenerate, repair or replace damaged tissues. A key challenge in this field is the ability to control cell organization, which is essential for the functionality of anisotropic tissues, such as cardiac tissue. Acoustic manipulation has emerged as a non-invasive, label-free and high-resolution technique to align cells and spheroids.

This dissertation explores the alignment of Human Dermal Fibroblasts (HDF) spheroids under acoustic fields, with the aim of developing an optimized setup for this purpose. The Six-Sigma Methodology was implemented to identify customer requirements, translate them into measurable parameters, analyse them and design possible concepts. The different factors that influence the acoustic field were studied through experiments with both microparticles and spheroids, whose movement was assessed using different software tools, such as ImageJ, Python, MATLAB and Microsoft Excel. In addition, amplitude measurements were conducted as a method to analyse losses of energy of the ultrasound waves after propagation.

The knowledge acquired from the experiments performed, regarding the influence of different parameters on the alignment of HDF spheroids, allowed the development of a House of Quality. Furthermore, design concepts for an optimized setup were developed in SolidWorks and pilot runs were conducted with the most promising alternatives. Additionally, a Design of Experiments was performed to evaluate the performance of the selected design.

This work advances the understanding of acoustic manipulation in tissue engineering, providing experimental insights, analytical tools and design strategies that support the development of more effective alignment systems.

Keywords: Acoustic Manipulation, Tissue Engineering, Alignment, Amplitude, Wave Propagation.

Contents

List of Figures

List of Tables

Methods and Materials

Implementation, Results and Discussion

Acronyms and Symbols

2D – Two-dimensional

3D – Three-dimensional

ARF – Acoustic Radiation Force

BAWs – Bulk Acoustic Waves

CAD – Computer-aided Design

CTQ – Critical to quality

DMADV – Define-Measure-Analyse-Design-Validate

DOE – Design of Experiments

ECM – Extracellular Matrix

HDF – Human Dermal Fibroblasts

IDT – Interdigital Transducer

KNN – K-Nearest Neighbour

PBS – Phosphate-buffered

PMMA - Polymethyl methacrylate

PZT – Lead Zirconate Titanate

QFD – Quality Function Deployment

RF – Radiofrequency

RMSD – Root Mean Square Deviation

ROI – Region of Interest

SAWs – Surface Acoustic Waves

TRIZ – Theory of Inventive Problem Solving

Z – Acoustic Impedance

p – Density

L – Distance between transducers

R – Fraction of energy reflected

f – Frequency

c – Speed of sound

λ – Wavelength

Chapter 1

Introduction

1.1. Dissertation Overview

This dissertation is structured into four main chapters. The present chapter introduces the field of tissue engineering, the importance of cell alignment and techniques for positioning cells, with emphasis on acoustic manipulation. The fundamental concepts of acoustic waves are described, followed by a literature review of experimental setups and recent advances in the field. Finally, the motivation and the goals of this work are presented.

Chapter 2 describes the methods and the materials. The main methodology was the Six-Sigma Methodology, and each step (Define, Measure, Analyse, Design, Validate) is briefly described. As this methodology follows an iterative approach, and in order to avoid redundancy while preserving the structural integrity of the dissertation, the methods of this work are presented in a general manner in this chapter, while specific details and experiments are described in Chapter 3.

Chapter 3 focuses on the implementation of the Six-Sigma Methodology, presenting and discussing the results obtained in each phase. Lastly, Chapter 4 discusses the conclusions drawn from these results, addressing the limitations encountered during this project, and outlines perspectives for future work.

1.2. Theoretical Background

1.2.1. Tissue Engineering

The field of organ transplantation has revolutionized the treatment of end-stage organ failure, improving patient survival and quality of life. As a result, the number of patients on transplant waiting lists has increased over the years. However, the availability of donor organs has not kept pace with this growing demand, making organ shortage a critical challenge in this field [1].

Tissue engineering is a field that has emerged as an optimistic solution to address this issue, since it relies on assembling functional constructs in vitro with the main purpose of regenerating, repairing and/or replacing biological tissues in vivo. Additionally, this field provides strategies for more accurate models to study diseases, consequently allowing more personalized treatments [2].

Tissue engineering relies on three essential components: cells, a structural support (scaffolds) and a prosperous environment for their growth [3]. It is important to mimic the conditions of natural body tissue to promote an efficient cell adhesion and proliferation, and therefore, the chosen scaffold should be structurally similar to the extracellular matrix (ECM) of the target tissue [4]. There are two main approaches for scaffolding. On the one hand, scaffolds can behave as structural supports for cells which are seeded onto them in vitro. Then, these cells generate ECM, forming the structural basis of a tissue

for transplantation. On the other hand, scaffolds can be combined with growth factors, and, upon transplantation, they attract cells from the body to the site, allowing tissue formation [5].

However, it is known that many scaffolds lack conductive properties and fibrous architectures, which are essential characteristics of the cardiac ECM, for example [6]. Thus, other approaches to accurately mimic tissue have also been studied and developed among the years. One of them is based on three-dimensional (3D) cell aggregates, such as spheroids, which may be used as a complement or as an alternative to scaffolding, since they resemble accurately the ECM. Spheroids have high cell density, allow cell-cell interactions and mimic cellular functions better than two-dimensional (2D) monocultures. Moreover, they have the inherent ability to fuse and act as building blocks for creating larger engineered tissues [7].

Spheroids have been studied in many fields of biomedical research, particularly in oncology. They have exhibited an increased drug resistance compared to 2D models, thereby mimicking the therapeutical resistance observed in real tumours more accurately than traditional monocultures [8]. However, for certain types of tissues, the full potential of spheroids depends not only on their biological characteristics but also on their spatial organization.

1.2.1.1. Cell Alignment in Tissue Engineering

For tissues where functionality is closely linked to structural anisotropy, such as neural, skeletal muscle and cardiac muscle tissue, the importance of having aligned cells is significant to ensure that specific functions are maintained [9]. For instance, the complex alignment of cardiomyocytes is essential for their ability to contract effectively [9, 10]. When this alignment is disrupted in the presence of a heart disease e.g., the contractile function is compromised, impairing its ability to pump blood to the whole body [10].

To replicate the natural level of organization in engineered tissues, several strategies have been developed to induce cell alignment in vitro. Hydrodynamic alignment techniques rely on controlled fluid flows to guide cellular orientation, which can be achieved by microfluidic channels or pipetting-based systems for example. Although these techniques are effective for 2D cultures, they generally lack ability to achieve full 3D spatial control [8].

Bioprinting offers a more direct method of positioning cells, mainly through extrusion-based or droplet-based printing. However, this technique lacks reliability, requires careful optimization of printing parameters for each tissue [8] and is limited by resolution [11].

Another technique to position microtissues relies on the modification of the substrate, either structurally by creating topographic features, or chemically to create cell-adhesive or cell-repellent regions. It has shown to be a simple and low-cost technology, but it is limited by the characteristics of the microtissue, and each new design requires the fabrication of a different mould [8, 11].

On the other hand, acoustic and magnetic forces allow for the positioning of microtissues without direct contact. These approaches are faster and less invasive than the ones previously mentioned [8, 11]. However, magnetophoresis requires the use of magnetic particles to label the microtissues, which may interfere with cellular function and behaviour [8]. In contrast, acoustic manipulation allows the migration of particles or cells under the influence of acoustic waves, without any need for labelling or

surface modification. This technique can be used for different cell sizes and has the potential to create microtissues of high cell density from a low number of cells [8, 12]. Furthermore, it offers high resolution, which is important to replicate complex aligned tissues [11, 12, 13].

For all these reasons, acoustic manipulation is increasingly favoured by different researchers, who believe that this technology is a promising tool to overcome the limitations of other strategies and has the potential to revolutionize tissue engineering [11, 12, 13, 14].

1.2.2. Acoustic Manipulation in Tissue Engineering

1.2.2.1. Acoustic Waves Propagation and Interaction

Acoustic waves are mechanical waves that travel through media by the vibration of particles. There are two types of waves based on their propagation direction: longitudinal waves, which propagate in the same direction as the vibration of the particles, and transverse or shear waves, in which particles vibrate perpendicular to the direction of propagation. While longitudinal waves propagate through gases, liquids and solids, transverse waves only propagate through solids since fluids can't resist to shear stress [15].

The propagation of sound waves is influenced by the mechanical properties of the medium, such as density and compressibility. When a wave encounters an interface between two different materials, part of it is transmitted, part is reflected and if the angle of incidence is not null, part of the wave may also be refracted. The ratio of the transmitted and reflected waves depends on the acoustic impedances (Z) of the two materials, which is a physical property that describes the resistance to propagation of sound waves [15, 16]. It is defined as the product of the density (p) and the speed of sound (c) of a material $(Z = pc)$. At an interface between two materials, if the wave strikes the surface at a right angle, the fraction of energy that is reflected (R) is defined as:

$$R = \frac{(Z_1 - Z_2)^2}{(Z_1 + Z_2)^2}, \qquad \text{(Equation 1.1)}$$

where Z_1 and Z_2 are the acoustic impedances of material 1 and 2, respectively [17].

High acoustic impedance mismatches between materials cause more reflection and less transmission of the wave, and therefore choosing the appropriate materials is an important decision when working with ultrasounds in tissue engineering.

In addition to acoustic impedance, acoustic attenuation is another physical property of materials that influences the propagation of sound waves. It is defined as the reduction of sound intensity as the wave travels through a medium, and it happens due to absorption and scattering. Absorption occurs when acoustic energy is converted into other forms of energy, such as heat, while scattering refers to the redirection of sound waves when they encounter an obstacle or heterogeneities within the medium [15]. When high amplitude acoustic waves are absorbed, fluid flows are induced in the direction of propagation, a phenomenon known as acoustic streaming. These flows induce a drag force on particles to move or rotate them, thereby influencing their original trajectory [18].

1.2.2.2. Acoustic Standing Waves

Acoustic manipulation, as mentioned, allows the organization of cells into structured patterns without direct contact. When two acoustic waves of the same wavelength are travelling in opposite directions, such as through reflection, a standing wave is created. This wave is confined in space but oscillates in time, creating regions of maximum pressure - antinodes, and minimum pressure – nodes [12], as seen in Figure 1.1.

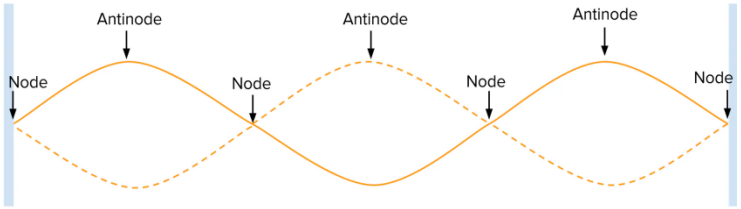

Figure 1.1 – Schematic of a standing wave [19].

As particles encounter this acoustic standing wave, they experience forces due to pressure gradients and tend to move towards an equilibrium position where their weight compensates the acoustic radiation force induced on their surface. This equilibrium position depends therefore on these particles' weight – particles smaller than half the wavelength $\left(\frac{\lambda}{2}\right)$ become trapped on nodes and particles in other size ranges tend to become trapped near the antinodes [20]. Based on this principle, it is possible to align and pattern particles or cells, as shown in Figure 1.2 [21].

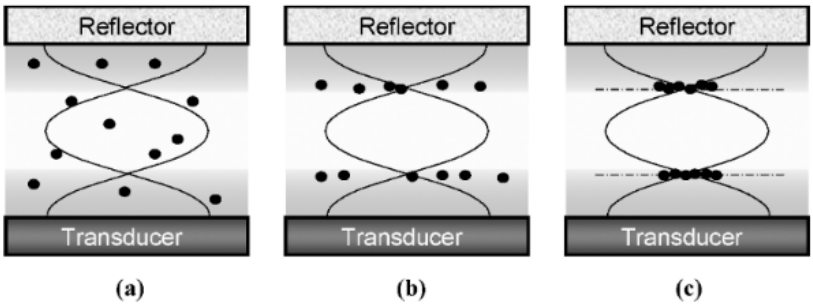

Figure 1.2 - Alignment of particles on node positions. (a) Creation of standing wave, (b) particles move towards the nodes, and (c) they align in bands. Adapted from Hill & Harris [21].

For particles smaller than $\frac{\lambda}{2}$, the acoustic radiation force (ARF) applied on each particle can be determined by the Gor'kov theory, which states that this force F is calculated by:

$$\vec{F} = -\nabla U, \qquad \text{(Equation 1.2)}$$

where U is the Gor'kov potential, given by:

$$U = 2\pi R^3 \left[\frac{\langle p^2 \rangle}{3pc^2} - \frac{p\langle u^2 \rangle}{2}\right], \qquad \text{(Equation 1.3)}$$

where R is the radius of the rigid particle, $\langle p^2 \rangle$ and $\langle u^2 \rangle$ are the time average of sound pressure and velocity squared, respectively, p is the density of the medium and c is the sound velocity in the medium [22].

This formulation proves that the ARF applied on a particle depends on the size of the particle, the properties of the media and the characteristics of the acoustic field. The Gor'kov potential allows a better understanding of particle movement under acoustic forces and is therefore important to be considered in the context of acoustic manipulation.

1.2.2.3. Types of Acoustic Waves

Acoustic manipulation in tissue engineering relies mainly on two types of ultrasound wave propagation: surface acoustic waves (SAWs) and bulk acoustic waves (BAWs).

In the first approach, an interdigital transducer (IDT) converts an electrical signal into a mechanical wave by inducing the vibration of a piezoelectric element, most commonly lithium niobate ($LiNbO_3$). This way, SAWs are created and travel along the surface of this element [12]. To create a standing SAW, at least one IDT and a reflector or two IDTs are needed, and different patterns can be achieved by changing their position, as shown in Figure 1.3. Some setups were also developed with four IDTs to generate two standing waves that interact with each other (Figure 1.4) [14].

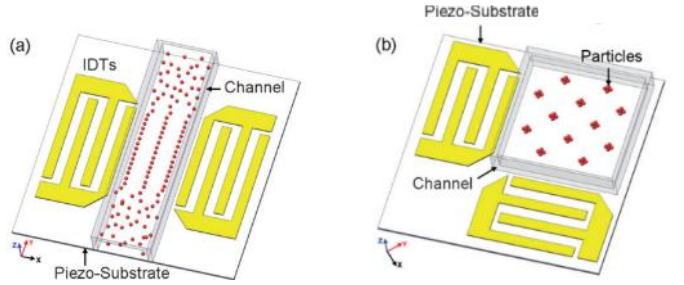

Figure 1. 3 - SAW devices. (a) 1D patterning device and (b) 2D patterning device. Adapted from Shi et al. [23].

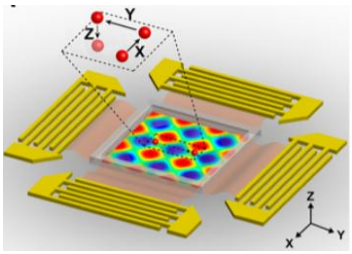

Figure 1.4 - SAW device with four IDTs for 3D patterning. Adapted from Guo et al. [14].

SAW devices are especially suited for being integrated within microfluidic devices or lab on a chip approaches due to their small scale, but they are not suitable for manipulation at a macroscopic scale [12].

On the other hand, BAWs propagate through the bulk of a material and are generated mainly by a lead zirconate titanate (PZT) transducer. This transducer converts a radiofrequency (RF) signal into a mechanical one, transmitting the acoustic wave through a propagation material, often liquid or hydrogel. Standing BAWs can be created by two opposing PZT transducers or by reflection of a single wave, enabling particles or cells to align in parallel bands [12]. Similar to SAW devices, some BAW devices were also developed with two pairs of transducers, enabling 2D manipulation (along x- and y-axis), as illustrated in Figure 1.5. [24].

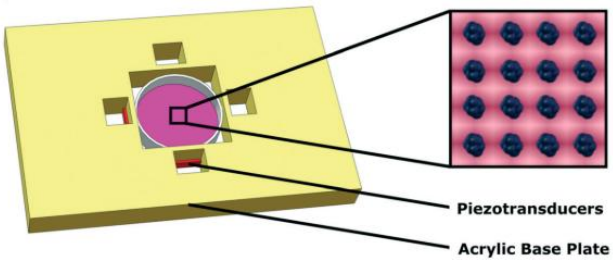

Figure 1.5 - BAW device with four transducers for 2D positioning of cells. Adapted from Armstrong et al. [24].

BAW devices, in contrast to SAW devices, allow patterning of larger areas and the use of standard labware, such as petri dishes. Although SAW setups are associated with higher resolutions, BAW setups are preferred when patterning spheroids and when operating with hydrogels or more viscous media [12].

1.2.2.4. Factors that Influence Alignment

As mentioned previously, the movement of particles by acoustic manipulation depends essentially on their physical characteristics, the characteristics of the medium and the properties of the acoustic field, and therefore so does their alignment.

The size, shape and density of particles influence their behaviour under acoustic fields. Besides the ARF applied to each particle, there is also a secondary force that acts between particles, which is especially important when they are in close proximity to each other, since it causes both attractive and repulsive forces. This secondary force has not yet been studied in detail, but a study developed by Zheng and Apfel [25] showed that it depends on the relative orientation of the particle pair to the wave propagation direction [26]. Although there is still no full comprehension of how particles movement is affected by this force, it is evident that the concentration of particles in the medium also plays a significant role in influencing alignment outcomes.

Properties of the medium, such as its density, sound speed and viscosity influence particles movement, as these directly affect acoustic impedance, attenuation and streaming. Materials with high viscosity attenuate acoustic waves fast due to acoustic damping. Additionally, materials with irregular surfaces may distort the acoustic wave and impact node positions. Adherent surfaces may also promote cell-attractive interactions, inhibiting cellular movement [24]. For these reasons, the type of propagation materials used should be carefully considered to optimize alignment [15].

The acoustic field originates from a transducer that receives an electrical signal with a specific voltage and frequency. This signal causes the piezoelectrical material to expand and contract, producing pressure changes that propagate as acoustic waves [27]. The characteristics of these waves, such as amplitude, frequency and direction, depend therefore on the input signal, on the type of transducer and its sensitivity, and on its position. Piezoelectric transducers respond with maximum output amplitude when they are driven at specific frequencies, known as resonant frequencies [17]. These resonant frequencies can be determined by an impedance analysis, as they correspond to minimum values of impedance [28].

The wavelength (λ) of an acoustic wave is determined by the following equation:

$$\lambda = \frac{c}{f} \qquad \text{(Equation 1.4)}$$

where c is the velocity of sound in a specific medium and f is the frequency of the acoustic wave [17].

The velocity of sound in a given medium is fixed and therefore the wavelength is inversely proportional to the frequency. For this reason, standing waves with higher frequencies have lower wavelengths, which translates to smaller distances between nodes and thus narrower spacing of aligned cell bands.

In a standing wave, the distance between the transducer and the reflector, or between the two transducers, is also relevant, since there is attenuation of the amplitude over long distances. Resonance occurs when the distance (L) between them is optimal, typically when it satisfies the following condition [29]:

$$L = n.\frac{\lambda}{2}, \quad n = 1, 2, 3 \ldots \qquad \text{(Equation 1.5)}$$

This distance ensures the waves are exactly in phase, and therefore their amplitudes add up, in a process known as constructive interference [17]. As a result, the amplitude of the standing wave is maximized.

1.2.2.5. Experimental Setups and Limitations

Many acoustic devices for cell alignment have been developed with different configurations and materials. In 2015, Scholz et al. [30] developed a setup with a pair of opposing PZT transducers separated by a cavity where particles and a medium were inserted. Both transducers were fixed against a polymethyl methacrylate (PMMA) wall by a spring. This device was able to align the majority of both spherical and cylindrical particles of different sizes, but it was noted that some particles remained stationary and unaffected by the acoustic field, probably due to frictional effects and secondary bonding to the substrate. It was also stated that PMMA introduced additional damping to the system [30].

In 2018, Armstrong et al. [11] created a BAW patterning device with two pairs of piezotransducers glued to an acrylic surface and a cavity for a petri dish. They exposed myoblasts to a 2.0-2.1MHz acoustic field for 30 minutes and proved that it didn't cause any prejudicial effect on their biological functioning. They also showed that these parameters can be used to pattern myoblasts within different hydrogels, leading to the formation of dense muscle fibers with anisotropic mechanical properties. As future work, they proposed the integration of a vertical standing wave to levitate myoblasts for the assembly of 3D fibers [11].

A year later, this device was again studied by Armstrong et al. [24] with the aim of developing a spatiotemporal method qualification of cell patterning. They used confocal fluorescence microscopy to capture clusters of cells and used Voronoï Tessellation as an image analysis tool. This method uses localized points in space to generate a set of tessellated polygons. Each polygon contains one point, and its boundaries are equidistant between two or more points, which means that all locations within a polygon are closer to its central point than to any other. Voronoï Tessellation allowed the extraction

over time of quantitative values, such as cluster density, number, area, barycentre and proportion of clustered seeds, which were helpful to assess the quality of patterning with different experimental conditions. For instance, they showed that tight clusters were formed around the resonant frequency, while disperse clusters were seen with other frequencies. Additionally, the analysis of clustered barycentre coordinates across different voltages revealed that higher voltages resulted in clusters placed at node positions. They concluded that Voronoï Tessellation is a simple, unbiased and informative method for quantifying the cell patterning process [24].

Chen et al. [31] in 2023 developed an acoustofluidic device in PMMA with a pair of parallel PZT transducers and with a central cavity to house cell culture medium. Spheroids were suspended in phosphate-buffered saline (PBS) and placed in a cell culture dish to avoid contamination. The voltage range imposed on the transducers was 5-15.3 volts peak-to-peak (V_{pp}) and their resonant frequency was 1.05MHz. They aligned and controlled interactions between spheroids successfully [31].

In the current year, Meng et al. [32] studied how geometric parameters of a circular transducer array affect the acoustic field and the trapping performance. The device consisted of 64 piezotransducers arranged around a circular water chamber with a matching layer on the inner surface and a backing layer on the outer surface of the piezoelectric elements. They determined the optimal impedance (z_m) and thickness (t_m) of the matching layer, which was made of 32% alumina and 68% epoxy, based on the following equations:

$$z_m = \sqrt{z_w z_{pzt}}\,, \qquad \text{(Equation 1.6)}$$

$$t_m = \frac{\lambda_m(2n-1)}{4}, \qquad (n = 1,2,3\ldots), \qquad \text{(Equation 1.7)}$$

where z_w is the impedance of water, z_{pzt} the impedance of the transducer and λ_m the wavelength of the matching layer [33].

The backing layer was made of 64% tungsten and 36% epoxy with an impedance matched to the piezoelectric layer to attenuate undesired waves. They studied the effect of water height on the acoustic pressure field and for a given piezo element height, they identified the water level that allows resonance and potentially improves trapping. Additionally, they examined the effect of the thickness of the bottom glass layer and concluded that thin layers have low pressure near the bottom, while thicker layers have high pressure, which is ideal for particle manipulation. They also studied the effects of the radius of the device and the number of elements on the pressure fields. All these simulations were consistent with experiments, which confirmed that higher pressure leads to better particle trapping [32].

1.3. Motivation and Objectives

The ability to control the spatial distribution of cells is essential in tissue engineering, as it improves the functionality of engineered constructs. Acoustic manipulation has proven to be a powerful tool for patterning and trapping cells and spheroids in a non-invasive way, while preserving their biological functions. The devices described previously have highlighted how careful the selection of materials, transducer arrangement and driving conditions should be to optimize alignment outcomes.

Motivated by this prior work, the main goal of this project was to develop an acoustic manipulation setup optimized for the alignment of Human Dermal Fibroblasts (HDF) spheroids. To accomplish this, it was necessary to experimentally investigate how spheroids behave under an acoustic field, and which parameters influence their behaviour. In the laboratory where this work was carried out, an acoustic alignment setup was already in use. However, it exhibited limitations, such as in terms of practicality and stability, which affected alignment consistency. This existing setup was studied experimentally to identify and characterize its shortcomings, and based on these insights, as well as on previous reported studies, the requirements for an improved setup were determined.

Overall, this project aimed to gather knowledge on spheroid alignment under acoustic fields, contributing to future experimental work in the field of tissue engineering.

Chapter 2

Methods and Materials

2.1. Six-Sigma Methodology

When developing new products or processes, it is important to have a structured approach to ensure customer needs are met. Define-Measure-Analyse-Design-Validate (DMADV) is a Six-Sigma methodology useful in this context, since it ensures that every phase of the development is accomplished. The Define phase focus on identifying project goals and customer requirements. The Measure phase involves gathering relevant data to quantify requirements and assess current capabilities. Next, in the Analyse phase, different design concepts that fulfil the requirements are evaluated and the best one is converted into a prototype in the Design phase. Finally, this prototype is tested and validated for its intended purpose [36].

In the present work, the DMADV methodology served as the main framework for the development of a strategy to improve spheroids alignment through acoustic manipulation.

2.1.1. Define Phase

As mentioned, the first step of DMADV is to define project goals and identify customer requirements, either through surveys, questionnaires, or analysis of previous complaints. In this context, customer needs were identified through conversations with researchers from the Duarte Campos Lab who have been studying this technology and who explained the limitations of the existent setups. Additionally, simple experiments were conducted to allow a better understanding of the behaviour of the current devices. For these experiments, microparticles were placed in Sarstedt chambers and their movement was seen through the stereo microscope when an acoustic field was present.

2.1.2. Measure Phase

In this phase, the customer requirements were understood and critical to quality (CTQ) measures were developed, which means the customer needs were translated into measurable product requirements. The Kano Model was useful in distinguishing between different types of customer requirements and in determining the level of importance that should be given to each one. The Kano Model outlines five types of customer requirements. Must-Be requirements are the fundamental features that customers expect, and their absence leads to dissatisfaction, while their presence does not increase satisfaction. One-Dimensional requirements, also known as performance features, are the ones that are directly proportional to customer satisfaction. Attractive requirements are not expected by the customer but can significantly enhance their satisfaction when present. On the other hand, Indifferent requirements refer

to the ones that don't impact satisfaction, while Reverse requirements are those whose presence leads to dissatisfaction, since they might go against customer expectations or preferences.

After distinguishing the different types of requirements, the quality drivers, i.e., the elements that drive quality for customers, were established, and the performance requirements (or CTQs), that ensure that each quality driver is met, were determined. Then, after all CTQs were identified and prioritized, it was also established an accurate measurement system for each one, to ensure that, when the time comes, it is possible to assess whether performance meets or not the initial requirements.

2.1.3. Analyse Phase

The Analyse phase is focused on analysing different design concepts for each CTQ. For that, Quality Function Deployment (QFD) was implemented, guiding the translation of customer requirements into design specifications.

This phase also included exploratory experimental work to gain insight into system behaviour under different conditions. The conducted experiments during this phase were performed to evaluate parameters that affect the acoustic field and alignment quality, providing important input to support design decisions.

2.1.3.1. Quality Function Deployment

The QFD process, often visualized through the matrices of the House of Quality, is divided into 4 phases and their matrices: product planning, product development, process planning and production planning. The first matrix was completed, and it was focused on assigning an importance of accomplishment to each quality driver, a target value for each CTQ and analysing the relationships between CTQs and quality drivers. Then, the CTQs were translated into product features in the second matrix, where target values were also assigned and relationships between features were established. The third and fourth matrices were not developed as the project was mainly focused on obtaining a conceptual understanding and performing early testing, without proceeding to full-scale fabrication.

The development of the QFD matrices was an iterative process that evolved throughout the project, with modifications made as new insights and findings emerged. For this reason, the results regarding this step are presented after the results of the other analyses.

2.1.3.2. Experimental Analysis

In this phase, experiments were conducted to better understand how different factors influence alignment. Three main approaches were defined and evaluated throughout this project. One was based on analysing the behaviour of microparticles under an acoustic field with different inputs, particularly their alignment time and wave distortion. As mentioned earlier, the aim of this project was to develop an optimized setup for the alignment of HDF spheroids. However, microparticles were used in specific

experiments due to their ease of handling and the lack of special preparation required. The use of microparticles in this stage was adequate because these experiments were mainly conducted to evaluate how the acoustic field changes under different conditions.

Another approach relied on amplitude measurements as a way to evaluate the acoustic energy loss and the strength of the acoustic field. Finally, the last approach was used in the final experiments and was based on the spheroid's behaviour, including their displacement and speed of movement, under different conditions.

The parameters that were considered to influence the acoustic field and the alignment of particles and spheroids, and that were therefore studied in this work, were: the frequency and the input voltage of the signal; the type of propagation medium and material; the volume of particles; the distance between transducers; the type of transducers; the water levels; the size of the chamber and the adhesion forces.

2.1.3.3. Design Concepts

Based on the results of the experimental analysis, different design concepts were conceptualized. The Theory of Inventive Problem Solving (TRIZ) was a useful tool in this context, since it is a systematic method for ideation that provides a set of principles for resolving design problems and contradictions.

After establishing different design solutions, each alternative was evaluated to determine the most suitable one. For this purpose, the Pugh Matrix was implemented, which is a tool that allows the comparison between proposed solutions and a baseline - typically a previous validated design. First, the characteristics that the final design should have were listed and weighted with a relative importance (0 – least important; 10 – most important). Then, each alternative was assessed, evaluating how well each option meets the defined characteristics in comparison to the baseline. This evaluation was made by assigning a score of -1 (if it appeared worse than the baseline), 0 (equal to baseline) or +1 (better than the baseline). Finally, the sum of ratings was calculated, allowing for the selection of the best design alternative.

2.1.4. Design Phase

In this phase, concepts were prototyped, and pilot runs were performed to evaluate their performance. A comparison between alternatives was established to experimentally conclude which one provides the best outcomes. Then, the selected alternative was evaluated through a Design of Experiments (DOE) to investigate its behaviour under different conditions.

2.1.5. Validation Phase

The Validation Phase was initially planned as the final step of the Six-Sigma methodology to confirm the performance and robustness of the selected design. This phase would typically involve

repeating experiments under controlled conditions, assessing reproducibility and confirm if all established requirements are met.

However, due to time constraints within the scope of this project, this phase could not be carried out experimentally. Instead, validation is addressed in Chapters 3 and 4, where the limitations of the study and potential strategies for future work are outlined.

2.2. Materials

2.2.1. Experimental Setups

The experimental setup present in the laboratory was composed by a signal generator (MFG-2230M, GW Instek), a high-power amplifier (LZY-22+, Mini-Circuits) with a 200× voltage gain, and an acoustic manipulation device. This device was designed to hold either a 35 mm diameter petri dish or a 25.5 mm wide chamber slide, as shown in Figure 2.1. It was 3D printed in tough resin (Blu, Siraya Tech) and two piezoelectric transducers (M165D25, Pro-Wave Electronics) with a diameter of 25 mm were glued to the resin supports. For experiments, this device was placed inside a rectangular chamber (63 × 95 mm), also 3D printed in resin, with a glass bottom glued to its base, as represented in Figure 2.2, which could hold water or other propagation media.

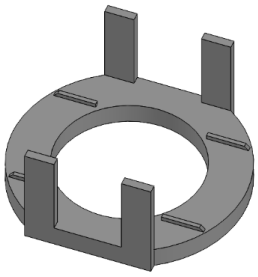

Figure 2.1 - Computer-aided design (CAD) of the resin support for petri dish or slide.

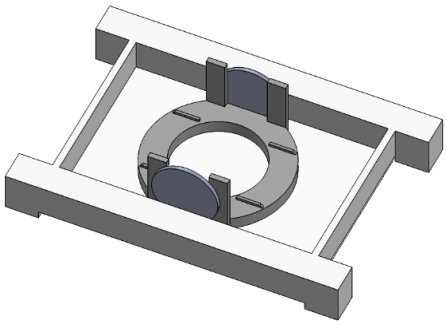

Figure 2.2 - CAD of the acoustic manipulation setup.

This setup was used for most of the experiments conducted at the ZMBH by the Duarte Campos research group, but due to its limitations, which are discussed in Chapter 3, an alternative transducer type was studied in this project. The resin support was the same as before and two rectangular (40×2×5 mm) PZT transducers (PIC181, Pi Ceramic) were glued to it, as shown in Figure 2.3.

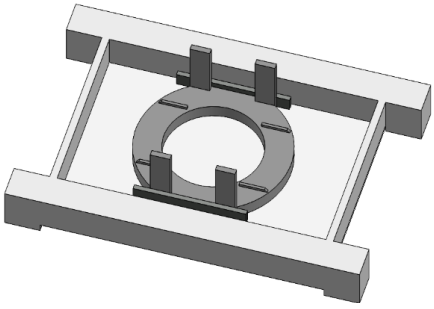

Figure 2.3 - CAD of the acoustic manipulation device with two PIC181 transducers.

The main difference between M165D25 and PIC181 was their resonance frequency. The M165D25 has a documented resonance frequency of 1.65 ± 0.05MHz, whereas the PIC181 does not have a specified resonance frequency. Instead, its resonance frequencies were determined by Dr. O'Dwyer Lancaster-Jones (Duarte Campos Lab, ZMBH) via an impedance analysis and are presented in Table 2.1.

Table 2.1 – Determined resonance frequencies of PIC181 transducer

Resonance frequencies	**PIC181 transducer**
f_{s1}	0.34 MHz
f_{s2}	0.97 MHz
f_{s3}	1.17MHz

In addition to these two setups, there was also a third design, which was based on Armstrong et al. [29], but with only a pair of piezo transducers (PIC181) and with a cavity for a chamber slide, as shown in Figure 2.4. This design was both 3D printed in resin and fabricated in plexiglass, or PMMA. In both versions, the transducers were glued to 2.10 mm tick walls and positioned 46.2 mm apart.

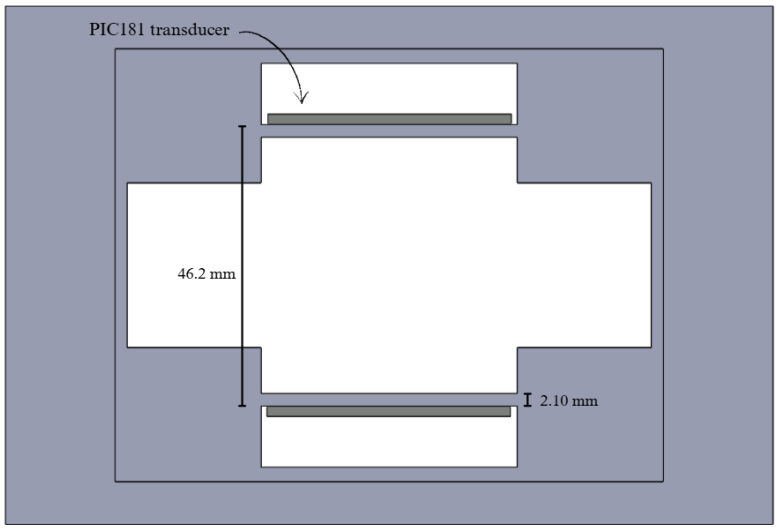

Figure 2.4 - CAD of acoustic device inspired on Armstrong et al. [29]. It has two PIC181 transducers glued to the walls and a cavity for a slide in the middle.

A summary of all acoustic devices that were available at the laboratory is presented in Table 2.2.

Table 2.2 - Different acoustic setups available at the ZMBH and their characteristics.

	Setup A	**Setup B**	**Setup C**	**Setup D**
Design description	Support for a petri dish or a chamber slide. It can be placed inside a rectangular chamber with a glass bottom (Figure 2.2)	Support for a petri dish or a chamber slide. It can be placed inside a rectangular chamber with a glass bottom (Figure 2.3)	Based on Armstrong et al. [29] with only a pair of transducers (Figure 2.4)	Based on Armstrong et al. [29] with only a pair of transducers (Figure 2.4)
Distance between transducers	50.0 mm	50.0 mm	46.2 mm	46.2 mm
Type of piezo transducers	M165D25	PIC181	PIC181	PIC181
Material of support	Tough resin	Tough resin	Tough resin	PMMA

For all setups, each piezo transducer had two soldered jumper wires connected to its positive and negative electrodes. These wires were then connected to a breadboard, which was linked to the amplifier and signal generator circuit, as illustrated by Figure 2.5. In the signal generator, the frequency and the voltage, which would then be amplified by 200×, were specifically defined for each experiment.

Figure 2.5 - Scheme of the acoustic manipulation circuit. Composed by a signal generator, a voltage amplifier, a breadboard and a setup (A, B, C or D). Setup B is illustrated as an example.

In some experiments, when there was a need to measure the amplitude of a signal, an oscilloscope (2225, Tektronix) was also used.

The microparticles used in this project were a Copolymer Microsphere Suspension from Thermo Fisher Scientific, and had a diameter of 12 µm. The HDF spheroids (106-05A, Sigma-Aldrich) had a diameter of 200 µm and were cultured on a Fibroblast Growth Medium (116-500, Sigma-Aldrich).

In most experiments, particles and spheroids were placed in chamber slides. There were three different types of chamber slides that were used throughout the project: 8-Well Sarstedt slides, 8-Well Ibidi slides and 4-Well Ibidi slides. The Sarstedt slides were the most cost-effective and had a removable frame, and for these reasons were only tested with particles in preliminary experiments. The 8-Well Ibidi slides were tested with both particles and spheroids, while the 4-Well Ibidi slides were only tested with spheroids at later stages of the project.

2.1.2. Preparation of HDF Spheroids

When working with biological materials, it is important to follow standardized procedures to ensure cell viability. To thaw HDF spheroids, the fibroblast growth medium was first pre-warmed in a 37ºC water bath. The vial containing the spheroids was taken out of liquid nitrogen storage and placed in water bath until fully thawed. It was then dried, cleaned with ethanol and placed inside the hood. Once inside the hood, 1000 µl of HDF media was added to the vial with a micropipette. Then, spheroids were transferred into a 15 ml falcon tube with wide opening tips. The tube was centrifuged at 50×g (relative centrifugal force, rcf) for 3.5 minutes and then the supernatant was carefully aspirated. Subsequently, 600 µl of HDF media was added into the tube and the spheroids were resuspended by pipetting up and down. Finally, the desired amount of spheroid suspension was transferred into a petri dish or a chamber slide.

At later stages of the project, to improve spheroid mobility and reduce adhesion to the bottom of the chamber, two different pre-treatment strategies were tested before placing the spheroids. In some experiments, a thin layer of Agarose (A9539, Sigma-Aldrich) was applied to the bottom surface and in others, an Anti-Adherence Rinsing Solution (STEMCELL Technologies) was used.

2.1.3. Imaging Systems

The visualization of the experiments is essential to understand and analyse their results, especially in the context of this project, where the purpose is to align particles and spheroids. Therefore, two different technologies were used, depending on the goal of each experiment.

A stereo microscope from Leica was used in experiments that required the visualization of the full well, particularly when the aim was to observe general changes of particles and spheroids distribution without focusing on fine details. In contrast, in experiments that required higher magnification and the capture of images, an EVOS microscope (M5000, Thermo Fisher Scientific) was used. This microscope is digital inverted, and it was equipped with 4×, 10× and 20× objectives. It enabled the detailed observation of individual particles and spheroids, allowing a more precise analysis of their movement under the acoustic field.

2.1.4. Software Tools

Throughout this project, different software tools were developed to analyse measurements and captured images of particles and spheroids under an acoustic field.

ImageJ was used to perform a Voronoï Tessellation and obtain the polygon areas of particles over time. First, the *Find Maxima* function was used with a prominence value of 26 to detect local intensity maxima corresponding to the particle positions, generating a point selection. Based on these detected points, the *Delaunay Voronoi* plugin was applied in Voronoi mode to construct a Voronoï Tessellation, segmenting the image into regions associated with each particle. Next, a threshold was set between pixel values 1 and 255 to isolate the polygons and the result was converted into a binary mask. The *Erode* function was then applied to refine the polygon boundaries. Finally, the *Analyse Particles* function was executed to extract and summarize the polygon areas and centroids.

These results were imported to Microsoft Excel and a region of interest (ROI) was determined for each experiment. The number of particles that were inside the ROI was determined, as well as the mean value of their areas. Based on these results, a Python script was used to generate a plot of mean areas over time and adjust, through the *curve_fit* function, an exponential decay model of the form:

$$y(x) = ae^{-bx} + c \qquad \text{(Equation 2.1)}$$

From this plot, **time to align** was defined as the time at which 95% of the alignment was achieved. This was computed by resolving for x in the next equation:

$$y(x) = 0{,}05a + c \qquad \text{(Equation 2.2)}$$

Yielding the final expression:

$$x = -\frac{\ln(0{,}05)}{b} \qquad \text{(Equation 2.3)}$$

An indicator of alignment quality, **wave distortion**, was determined by a Python script that computed the vertical distribution of pixel intensities across the width of the image. For every column (x-coordinate), sampled in steps of 10 pixels, this script extracted the intensity profile within the ROI and calculated the vertical centre of mass. These centres were plotted to visualize the alignment profile, and the root mean square deviation (RMSD) of the centres from their mean value was calculated. A lower RMSD indicated a less distorted alignment of the particles.

These image analysis strategies developed for microparticles were not suitable for studying spheroids alignment due to differences in size. Therefore, a different script was developed in MATLAB to track spheroids' position over time. Each frame was first pre-processed by enhancing local contrast using *adapthisteq* function, followed by Gaussian blurring. The images were then binarized using adaptive thresholding and filtered to retain objects within a specified area range, corresponding to spheroid size (40 – 150 pixels of diameter). From this, the centroids of the spheroids were extracted, and a k-Nearest Neighbour (KNN) algorithm was applied to track individual spheroids across frames, linking centroids from one frame to the next. Based on the resulting trajectories, the script determined the **total displacement** (cumulative path length), **net displacement** (distance from initial to final position) and **average speed** (total displacement divided by the time taken) for each spheroid.

Additionally, a different Python script was used to process amplitude measurements as part of a parameter optimization experiment. The methodology and details of this strategy are presented in the next chapter.

A summary of the methods of this dissertation is schematized in Figure 2.6.

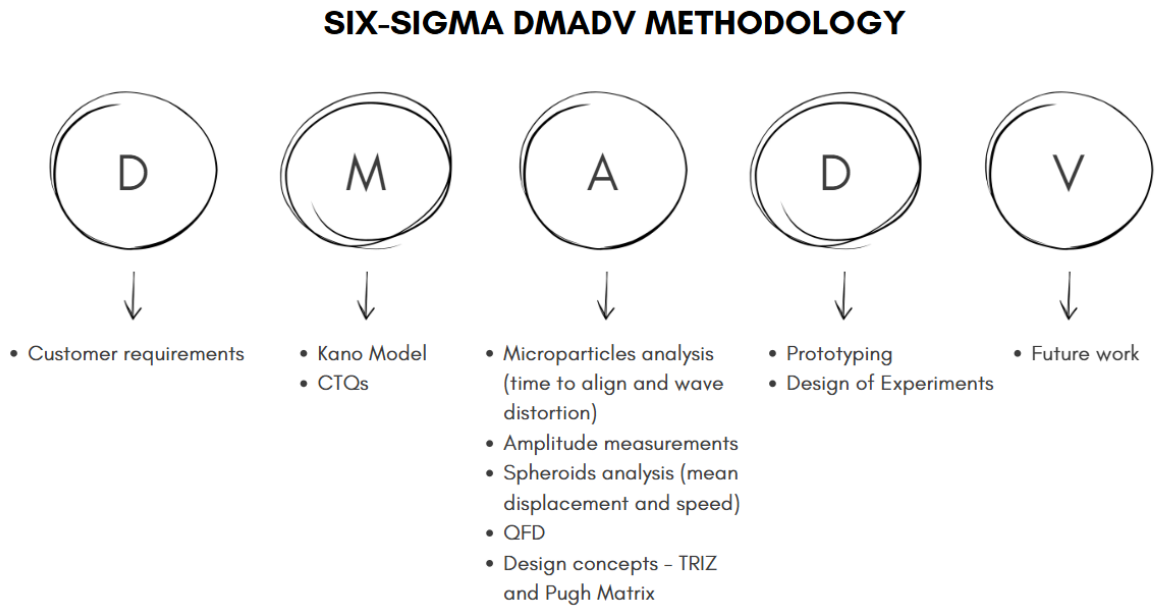

Figure 2.6 - Scheme of the Six-Sigma adopted methodology. For each phase, a summary of the steps taken is presented.

Chapter 3

Implementation, Results and Discussion

3.1. Define Phase

In this phase, customer requirements were mainly established based on researchers' opinions, who pointed out characteristics they desired in the setup and limitations of the current options. The main purpose of the setup was to provide a good alignment of spheroids using acoustic manipulation, and therefore one requirement was defined as "**Effective cell alignment**". Since the preparation of the spheroids should occur under sterile conditions, the setup needed to be **practical for hood testing**, as well as a **good environment for cell survival and growth** to ensure spheroids fuse and create large and complex structures that mimic tissue. This setup should also **allow visualization of results**, so it is possible to monitor and evaluate the quality of alignment, and be a **convenient design**, i.e., portable and stable to avoid alignment loss.

3.2. Measure Phase

In this step, the customer requirements were classified based on their type according to the Kano Model, as shown in Table 3.1.

Table 3.1 - Classification of the customer requirements.

Customer Requirement	Type of Requirement
Effective cell alignment	Performance
Practical for hood testing	Must-Be
Design convenient	Performance
Allows visualization of results	Must-Be
Good environment for cell survival and growth	Must-Be

"Effective cell alignment" and "Design Convenient" were considered performance requirements, since user satisfaction increases with their fulfilment. On the other hand, "Practical for hood testing", "Allows visualization of results" and "Good environment for cell survival and growth" were classified as must-be requirements because they are expectations that should be met to avoid customer dissatisfaction.

The quality drivers of each requirement and their CTQs were determined and are presented in Table 3.2.

Table 3.2 - Quality drivers and their CTQs established for each customer requirement.

Customer requirements	**Quality Drivers**	**CTQs**
Effective cell alignment	Effective signal emission	Initial amplitude of wave (V)
		Frequency (MHz)
	Efficient acoustic wave propagation	Amplitude after propagation (V)
	Precise and robust alignment	Number of spheroids in ROI (%)
		Wave distortion
		Direction of alignment (º)
		Deviation from initial alignment after disturbance (µm)
	Fast alignment	Time to align (s)
Practical for hood testing	Sterilizable	Thermal stability
		Ethanol resistance
	Ease of use inside of hood	Dimensions (mm)
		Shape
Design convenient	Portable without alignment loss	Dimensions (mm)
		Deviation from initial alignment after disturbance (µm)
		Weight (g)
	Mechanical robustness	Shape
		Structural rigidity
Allows visualization of results	Compatible with imaging techniques	Shape
		Light transmittance (%T)
Good environment for cell survival and growth	Can be placed in the incubator	Dimensions (mm)
		Thermal stability

An effective cell alignment requires an effective signal emission, which means that the signal sent by the signal generator and amplified by the circuit should be successfully converted to an acoustic wave

by the piezotransducer. This occurs when the transducer operates at its resonance frequency and the voltage at its terminals is similar to the input. Then, the ultrasound wave produced should propagate with minimum energy loss and refraction, and its efficiency can be assessed by measuring the amplitude of the wave after it travels through the medium, since it potentially reflects how much of the initial signal is preserved. The outcome of this system, i.e., the alignment, should be precise and robust. These characteristics can be measured by analysing the percentage of spheroids in a predefined ROI, which indicates the effectiveness of alignment; the wave distortion, which assesses the consistency of the pattern; direction of alignment, which evaluates the angle orientation of the aligned structures; and lastly how much deviation of the alignment occurs after a mechanical disturbance, to assess the robustness of the alignment over external influences. It is also relevant to have a fast alignment, since it reflects the system's responsiveness, and which can be measured by the time particles take to align.

A setup practical for hood testing should be sterilizable, which means it can be autoclaved and ethanol cleaned without compromising its stability and performance. It should also be optimized in terms of size and shape to facilitate easy handling inside the hood.

A convenient design setup should be portable without compromising alignment, meaning its dimensions and weight should allow easy transport while maintaining alignment stability and minimizing deviations after handling. Additionally, it should have an optimized shape and be structurally rigid to ensure its mechanical robustness, preventing its components from disassembling over time.

In this context of tissue engineering, it is important that the setup allows the visualization of the alignment outcomes. Therefore, it should have a high percentage transmittance (%T) of light and an optimized shape for it to be compatible with imaging techniques, such as the use of a microscope.

Finally, a setup that ensures a good environment for cell survival and growth should have the appropriate dimensions and maintain thermal stability, allowing it to be placed inside the incubator, which provides the optimal conditions for spheroids fusion and tissue development.

A measurement system for each CTQ was established, as shown in Table 3.3.

Table 3.3 - Measurement system for each CTQ.

CTQ	**Measurement system**
Initial voltage (V)	Measured with a voltmeter on transducers
Frequency (MHz)	Impedance analysis of transducers. Frequency sweep and amplitude measurement
Amplitude after propagation (V)	Measured signal amplitude with an oscilloscope at the receiving transducer
Number of spheroids in ROI (%)	ImageJ analysis of captured images
Wave distortion	RMSD of the centres of mass positions of particles
Direction of alignment (º)	Angle analysis from EVOS images
Deviation from initial alignment after disturbance (º)	ImageJ analysis comparing before and after disturbance
Time to align (s)	Time taken for particles to reach 95% alignment completion, through Voronoï Tessellation
Thermal stability	Exposure to 38ºC and a structural integrity check after autoclave
Ethanol resistance	Structural integrity check after ethanol sterilization
Dimensions (mm)	Measured with a calliper
Shape	Visual inspection
Weight (g)	Measured with a scale
Structural rigidity	Mechanical stress test
Light transmittance (%T)	Measured with a spectrophotometer

For the duration of this project, thermal stability, ethanol resistance, structural rigidity and light transmittance were not measured through these systems. However, the properties of the materials used were known, and visual inspections were conducted on the setups to ensure their adequacy.

It is also relevant to note that even though the aim of the project focused on spheroids alignment, CTQs like wave distortion and time to align were only measured using microparticles, since spheroids are wider, and an appropriate method to evaluate them was not developed within the scope of this work. Nonetheless, these CTQs served mainly as indicators of the strength and stability of the acoustic field, and therefore the use of microparticles to assess them was appropriate. In later stages, during the next phase involving spheroids, the strength of the acoustic field was instead evaluated based on spheroids displacement and average speed, as mentioned previously.

3.3. Analyse Phase

3.3.1. Preliminary Analysis

A preliminary experiment with Setup B (PIC181 transducers) was conducted to better understand how different frequencies affected alignment. This experiment was performed with microparticles in a Sarstedt slide and images were captured by the EVOS microscope after two minutes under an acoustic field. The input voltage was always the same, while frequencies were varied. Table 3.4 shows the values of the frequency tested.

Table 3.4 - Frequencies tested in Setup B. * indicates resonant frequency.

Frequencies (MHz)									
0.96	0.97*	0.98	0.99	1.00	1.15	1.16	1.17*	1.18	1.19

Figure 3.1. shows the alignment of microparticles under an acoustic standing wave with an initial amplitude of 22 V, using Setup B. The top images (A and B) correspond to the experiments performed with resonant frequencies – 0.97 MHz and 1.17 MHz, respectively. Images C and D illustrate the alignment at 1.00 MHz and 1.15 MHz. Images corresponding to other frequencies are included in Appendix A.

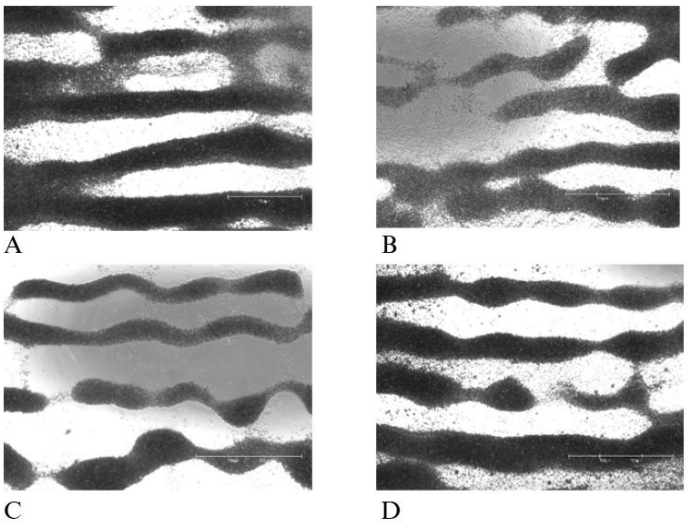

Figure 3.1 - 4x EVOS images of microparticles under an acoustic field of 22V. A – under a signal of 0.97 MHz; B - 1.17 MHz; C - 1.00 MHz; D - 1.15 MHz.

Although resonant frequencies are expected to provide a stronger acoustic field and therefore a better alignment, both Figures A and B show poorly defined bands with inconsistent directions of alignment. Among all frequencies tested, 1.00 MHz and 1.15 MHz produced the most well-defined, parallel alignment bands. The first resonant frequency of the PIC181 transducers (0.34 MHz) was not analysed by this method, since a simple test under a stereo microscope showed no effect on microparticles.

Altering the frequency of the signal shifts the position of the pressure nodes, and therefore the position of the bands. For this reason, instead of taking images on the exact same location for each experiment, the entire chamber was visually assessed under the EVOS microscope and images were taken from the region where alignment seemed most well-defined. This was performed as an initial evaluation to observe possible effects and provide insights into method development. This strategy is subjective and potentially biased, but it was considered the most appropriate way to evaluate and compare the effect of frequency on the alignment.

To note, the only change between these tests was the frequency of the signal. All experiments were performed on the same Sarstedt chamber and the number of particles, as well as the volume of water inside and outside the chamber, were always the same. This consistency allows for comparisons between tests. However, it is not possible to conclude which frequency is the absolute optimal, as different experimental conditions, such as a higher number of particles, could lead to different alignment outcomes.

Then, another experiment with Setup B was conducted to understand how the combination of different values of input voltage, frequency, type of propagation material and volume of particles affected alignment. In this experiment, the alignment quality was assessed by time to align and wave distortion. Images were captured using the EVOS microscope with the 10x objective every 5 seconds for over a period of two minutes. The images were captured in a region which was previously assessed and visually considered as the site that provided the more well-defined results. The tested values are present in Table 3.5.

Table 3.5 - Tested values of input voltage, acoustic refractive index of material, volume of particles and frequency of the signal.

Factor	**Low level**	**High level**
Input Voltage (V)	18.0	30.0
Acoustic Refractive Index (relative to water)	0.938 (Ultrasound Gel)	1.00 (Water)
Volume of particles (µl)	2.00	5.00
Frequency (MHz)	1.00	1.15

From the combination of these factors, 16 experiments were conducted. Table B1 in Appendix B shows the complete design and results. In six of these experiments, the Voronoï areas did not change over time, indicating that alignment would not occur. Therefore, time to align and wave distortion could not be determined in these cases. For the remaining experiments, both responses were calculated and then normalized using ceiling values, which were chosen to be higher than the largest result. Time to align was normalized by 300 s, since the largest determined result was 234 s. Wave distortion was normalized by 15 RMSD because the largest calculated RMSD was 11.9. In this context, a normalized value of 1 represents an inestimable response, whereas a value of 0 corresponds to optimal performance of each response. The effects of the four factors on time to align and wave distortion are represented in Figure 3.2.

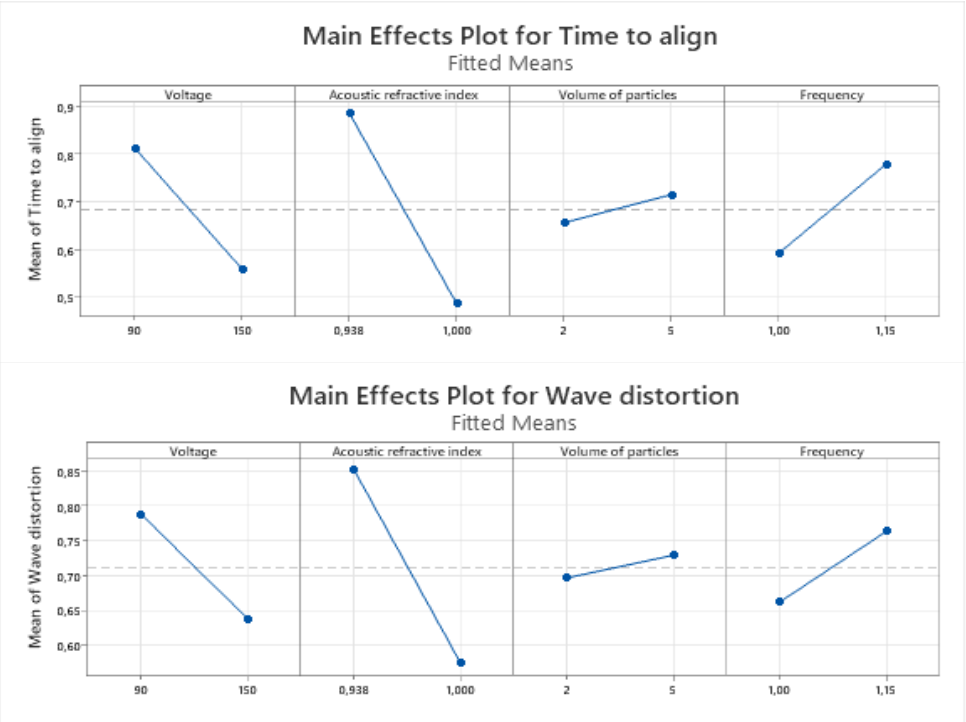

Figure 3.2 - Main effects of variables on time to align (top) and wave distortion (bottom).

Time to align and wave distortion exhibited similar trends in terms of how factors influenced them, indicating that conditions which reduced alignment time also reduced its distortion, and vice-versa. This suggests a strong relationship between these two metrics, possibly reflecting that a slower movement of particles is associated with a weaker acoustic field and, consequently, a less precise alignment.

Among all the factors, the acoustic refractive index seemed to have the greatest influence on both metrics, while the volume of particles had the least impact. Even though the ultrasound gel is used as the main coupling material in many medical applications, in this context water seemed to provide better results. This might be due to the presence of air bubbles in the gel, when it is not compressed against a surface, which could attenuate the acoustic wave. Additionally, during the experiments, it became evident that using ultrasound gel was less convenient and practical than water, as it required extra handling and more effort to clean the setup.

The effects of the interactions between factors on time to align and wave distortion were also analysed and are presented in Figure 3.3.

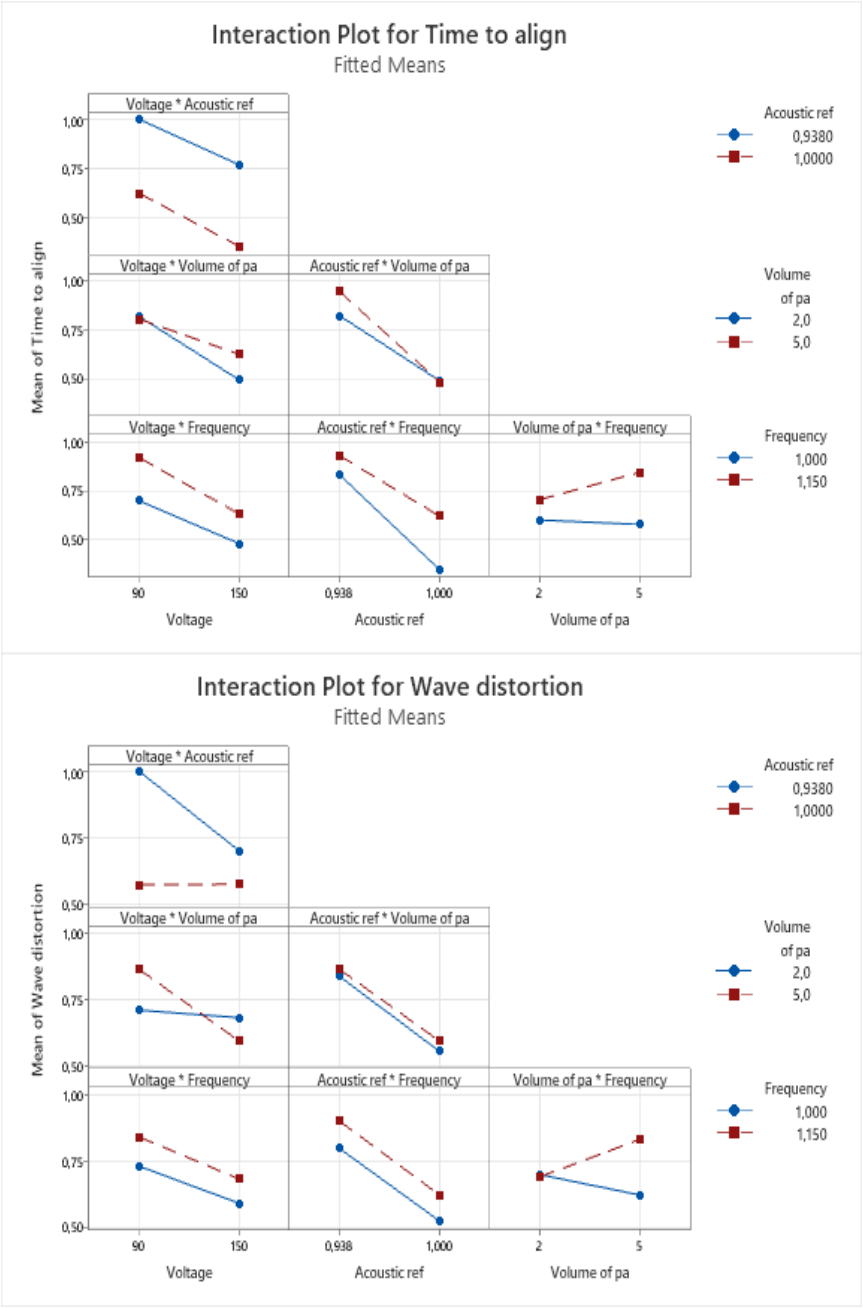

Figure 3.3 - Effects of the interactions between factors on time to align (top) and wave distortion (bottom).

Time to align and wave distortion exhibited similar trends. However, some differences were observed in specific factor interactions. Input voltage had a comparable effect on alignment time for both propagation materials, but it had a greater impact on wave distortion when ultrasound gel was used, whereas with water it had no apparent influence. Additionally, the interaction between the acoustic refractive index and the volume of particles on wave distortion is represented by parallel lines, which suggest little to no interaction effect. In contrast, these factors seem to interact in their effect on time to align. A similar pattern is also seen in the interaction between the refractive index and frequency. These findings suggest that the relationship between time to align and wave distortion is not strictly linear and may vary depending on the factor combinations.

In order to better understand how the interaction between factors influenced time to align and wave distortion, a Pareto Chart of the Effects was determined for each response, as shown in Figure 3.4. The reference line represents the threshold for statistical significance at a confidence level of 95% ($\alpha = 0.05$).

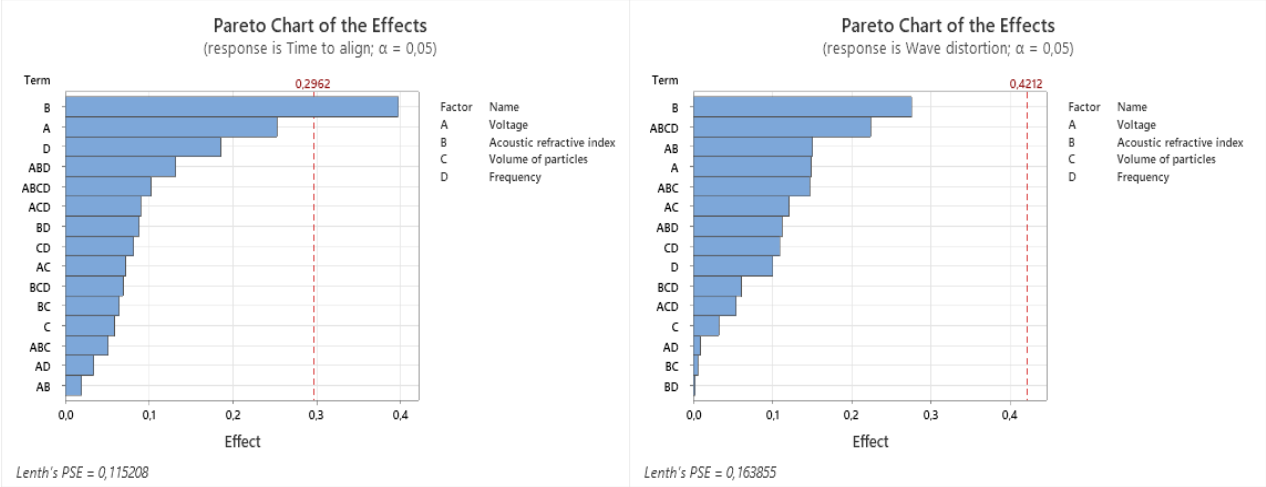

Figure 3.4 - Pareto charts of the effects for time to align (left) and wave distortion (right).

The acoustic refractive index was the only factor statistically significant, meaning that it potentially has a real impact on time to align. Although it also showed the largest effect on wave distortion, this influence was not statistically significant. It is important to note that each one of the 16 experiments was conducted only once, and thus, to increase the reliability of these conclusions, additional replicates would be necessary.

The approach adopted to normalize response values has some limitations. The ceiling values (300s for time to align, and 15 RMSD for wave distortion) were not determined but chosen to exceed the largest results. Assigning these values to inestimable runs allowed inclusion in factorial analysis but might have compressed differences among measurable runs and potentially inflated effects of some factors or interactions. An alternative approach would be to treat alignment as a binary outcome (achievable vs. unachievable) and analyse which factors affect alignment occurrence and which factors affect alignment timing and distortion. However, this would discard quantitative information and reduce the number of samples available for analysis.

3.3.2. Comparison Between Setups

Following the preliminary analysis, an experiment was conducted to assess the performance of three existing alignment setups in terms of loss of energy – setup B, C and D. The aim of this study was to determine which setup preserved the acoustic signal strength most effectively, since differences in material were expected to influence wave attenuation and, consequently, cell alignment. To investigate this, four experimental configurations were applied to each setup and the amplitude of the wave was measured as an indicator of energy loss. In the first configuration, only water was present in the setups. One transducer was connected to the signal generator and to the amplifier, serving as the emitter. The second transducer was connected to the oscilloscope, acting as a receiver. This way, an acoustic signal was emitted by the first piezo, and after propagation it was converted back into an electrical signal by

the receiving transducer. The resulting waveform was visualized on the oscilloscope and its amplitude was analysed.

In the second configuration, an 8-well Ibidi slide was introduced between the transducers, and the rest of the setup remained the same as before. For the third configuration, the receiving piezo was disconnected, and a third transducer was placed vertically inside a chamber of the slide and connected to the oscilloscope, allowing for the measurement of the amplitude directly at the point where spheroid alignment would later occur. The last configuration was similar to the third one, but both transducers from the setup were connected to the signal generator to create a bulk standing wave, while the vertical transducer was again the receiver.

In this experiment, three input voltages - 10 V, 20 V and 30 V, were tested at 1 MHz. Figure 3.5 shows the measured amplitudes of each setup for each experiment, and their linear regressions.

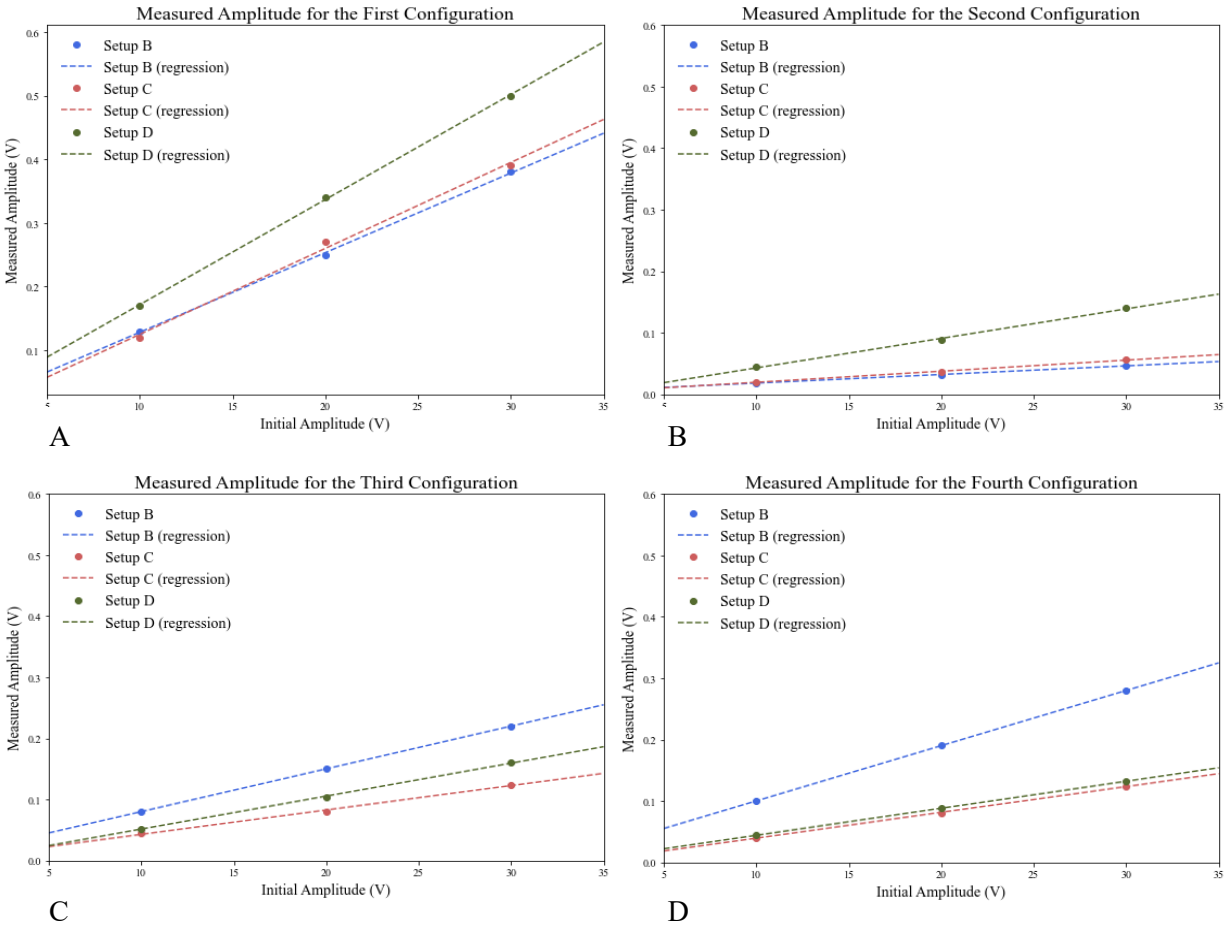

Figure 3.5 - Measured amplitudes in all four configurations, for each setup.

In the first configuration, Setup D provided the highest values of amplitude across all input voltages. Setups B and C yielded very similar amplitudes to one another, both lower than Setup D. Although Setup D has more material discontinuities, i.e. number of interfaces the wave must go through, than Setup B, the acoustic impedance mismatches might be lower. This may be attributed to the use of PMMA ($Z = 3.26$ MRayl), as a coupling material, which may offer better impedance matching between the PZT ($Z = 36.6$ MRayl) and the water ($Z = 1.48$ MRayl). Setup C has the same number of

discontinuities as Setup D, but tough resin has a lower acoustic impedance ($Z = 2.0$ MRayl) than PMMA, resulting in greater mismatches.

From Equation 1.1, it is possible to determine the fraction of energy that is reflected in these interfaces (Table 3.6).

Table 3.6 - Fractions of reflected energy (%) for each interface, obtained from Equation 1.1.

	Interface PZT - water	**Interface PZT – Resin**	**Interface PZT - PMMA**
Energy reflected (R)	85.1 %	80.3 %	70.0 %

The fractions of reflected energy obtained corroborate the measured amplitudes, justifying the differences between setups. A high reflection fraction is associated with a high loss of energy, i.e., loss of amplitude of the wave.

For the second configuration (Figure 3.5B), when an 8-Well Ibidi slide was placed inside the setups, a decrease in amplitude was observed for all setups. Setup D exhibited an average reduction of approximately 73%, Setup C decreased by about 85%, and Setup B by 87%. Despite this overall decrease, the relative trend remained consistent, with Setup D continuing to produce the highest amplitudes and Setups C and B providing lower and very similar results between each other.

In the third configuration (Figure 3.5C), the receiver transducer was placed vertically inside the closest chamber to the emitter. Opposite to before, Setup B produced the highest values of amplitude, while Setups C and D yielded similar results, especially for an input of 10 V. In this experiment, the area of reception of the signal was significantly smaller than previously, which likely influenced the outcomes. The presence of additional layers (PMMA in Setup D and resin in Setup C) may have introduced more wave refractions and scattering. As a result, the acoustic wave may not have been effectively directed into the desired receiving chamber but instead may have travelled through adjacent chambers until reaching the other transducer from the setup. This could explain the differences in trends between this configuration and the previous two.

In the fourth configuration (Figure 3.5D), amplitude was also measured inside the well, but a standing wave was created by the two transducers from the setups. In this case, Setup B was again the one that yielded the highest amplitudes. Setups C and D produced, once more, lower and very similar amplitudes between each other for all input values. Also, the differences between Setup B and the two other setups are greater than in the last configuration. A standing wave relies on constructive interference between acoustic waves from both transducers, and so refractions or distortions introduced by the layers of acrylic and resin could further reduce the amplitude measured in Setups C and D, explaining the results obtained. However, introducing a receiver transducer within a chamber where a standing wave is established may perturb the wave field due to scattering, therefore the results from this experiment should be only interpreted comparatively rather than as absolute measurements.

It is relevant to note that, for the last two configurations, it was challenging to place the receiver transducer exactly at the same location across all setups. Therefore, a position scan was always performed inside the chamber to identify the location that provided the highest amplitude. The receiver transducer was then fixed at that specific location of each setup. As a result, the position of the receiver varied between setups and configurations, but it was consistently chosen to maximize amplitude,

ensuring the most representative measurements. Additionally, it is important to mention that each experiment was conducted only once for each setup. Therefore, conclusions drawn from these results are not statistically reliable but were valuable for guiding future studies in the right direction.

The aim of this project was to improve the alignment of spheroids, and therefore the priority was to enhance the acoustic field inside the chamber where spheroids would be placed. Thus, additional experiments were conducted with the third configuration to achieve statistically reliable results. The third configuration was chosen over the fourth configuration, since it is expected to induce less wave distortion. The amplitude was measured seven times for each setup and each input voltage, and two frequencies were tested and compared – 1.00 MHz and 1.15 MHz. Figure 3.6 shows the measured amplitudes for each setup.

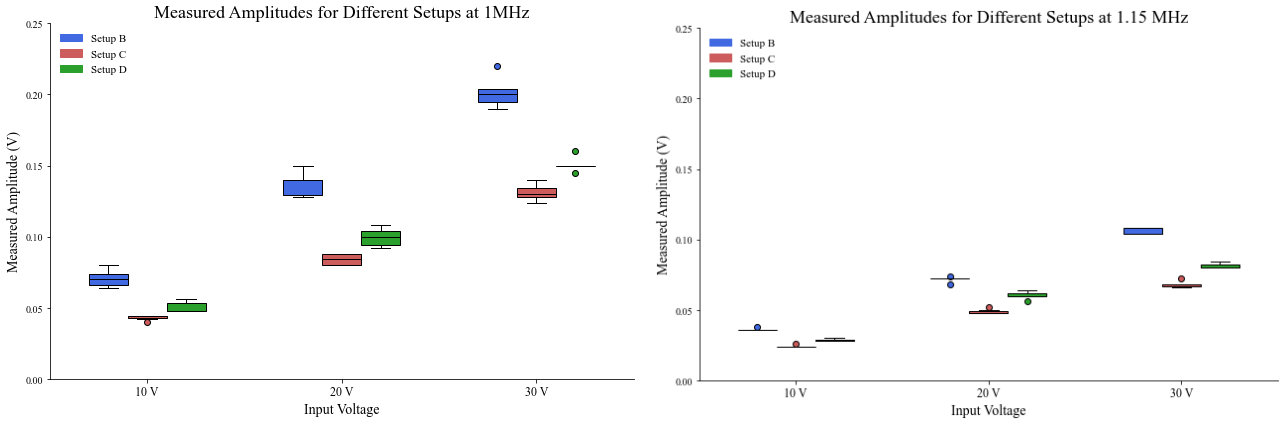

Figure 3.6 - Measured amplitudes for all three setups in the third configuration. A - At 1.0 MHz and B - at 1.15 MHz.

These measurements were carried out under different conditions from the previous ones, and factors such as the volume of water outside the chamber were not the same. Nonetheless, Figure 3.6 shows a trend similar to Figure 3.5C, where Setup B provides the highest amplitudes for all input voltages. In this set of experiments, after each of the seven measurements, the receiver transducer was slightly moved and a location scan was performed to identify again the spot yielding the highest amplitude, thereby ensuring reproducibility of the results.

It is possible to observe that neither Setup C nor Setup D achieved amplitudes inside the chamber as high as those of Setup B, for either frequency. A statistical analysis was performed to evaluate if these differences were significant. First, normality was confirmed for each setup at each input voltage using the Shapiro-Wilk test. Then, an F-test was applied to assess the equality of variances between setups for each input voltage, confirming homoscedasticity. Finally, ANOVA was performed to compare amplitude values between the setups, and no statistically significant differences were found for any input voltage at either frequency. This result may be attributed to limited sample size. To test this hypothesis, Sample *t*-tests were performed to determine the minimum number of samples required to determine significant differences with 80% power. The results of this analysis (Appendix C) showed that 7 replicates are not enough to detect differences between setups. Nevertheless, the observed trend of higher amplitudes in Setup B may still have practical relevance, especially to guide further experiments.

It is also possible to note the differences in measured amplitude between the experiments conducted at 1.00 MHz and the ones conducted at 1.15 MHz. The first ones reached a maximum of 220 mV, while at 1.15 MHz the maximum reached was less than 50% (108 mV). To understand if the differences between frequencies for each setup were statistically significant, a series of statistical tests was conducted. For each setup and each input voltage, normality was confirmed using the Shapiro-Wilk test,

and homogeneity of variances was validated with an F-test. Given that both assumptions were met, a Student's t-test was applied. Statistically significant differences ($p < 0.05$) were found in 8 out of 9 comparisons, indicating that frequency influenced amplitude for most conditions. The only combination that did not yield a significant difference was Setup D at 10 V ($p = 0.055$).

Thus, this analysis showed that the frequency of the signal has an impact on the amplitude of the wave, proving that 1.00 MHz allows a stronger acoustic field inside the chamber than 1.15 MHz, under these conditions. For this reason, further experiments were mainly conducted with 1.00 MHz.

3.3.3. Distance Between Transducers

The influence of the distance between transducers in the amplitude of the wave was evaluated. In this experiment, a PIC181 transducer was glued to a 1.10 mm thick glass and placed horizontally immediately after the resin supports of the setup, with the help of an XY-Stage, as shown in Figure 3.7.. This stage allowed the movement of the transducer towards the Ibidi slide, while maintaining a standing wave. This way, this transducer, as well as the opposite one from the original setup, were connected to the signal generator and amplifier circuit. The amplitude inside the chamber of the 8-Well Ibidi slide was measured with a vertically positioned PIC181 transducer connected to an oscilloscope, as illustrated by Figure 3.8.

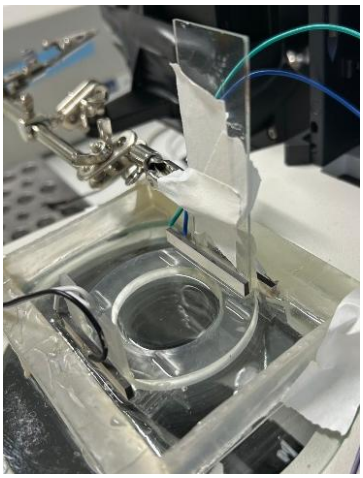

Figure 3.7 - Experimental setup composed by a PIC181 transducer glued to a glass, which is controlled by an XY-stage, inserted in Setup B.

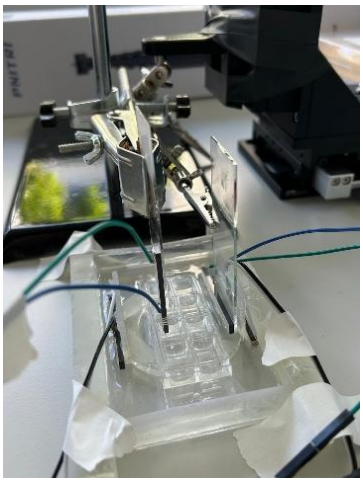

Figure 3.8 - Experimental setup for amplitude measurements. A PIC181 transducer was glued to a glass and placed vertically inside a chamber with the help of a universal support stand.

The amplitude was analysed continuously in the oscilloscope during the movement of the horizontally positioned transducer in Setup B. Three different input voltages were tested – 10 V, 20 V and 30 V – with a frequency of 1.00 MHz. The transducer glued to the glass was initially positioned right after the resin supports of Setup B, as shown in Figure 3.9.

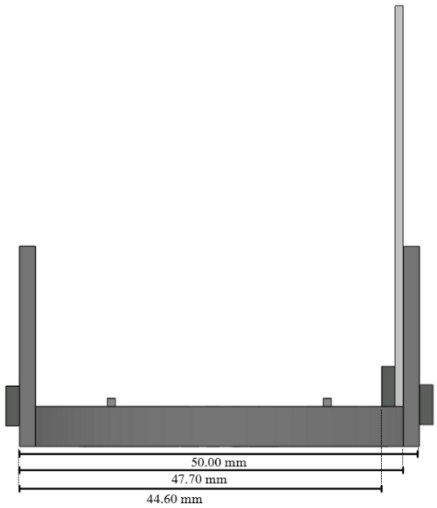

Figure 3.9 - Scheme of initial positioning of the setup (lateral view). The distances between components are represented.

The movement of the piezo revealed a periodic oscillation in the measured amplitude and therefore, the distances between the transducers that promoted maximum and minimum values of amplitude were recorded. These distances are referred to as the resonant distances of the setup and are presented in Table 3.7. Figure 3.10 illustrates the values of amplitude observed during the experiment with a spline interpolation applied to aid interpretation.

Table 3.7 - Resonant distances detected in the experiment.

Practical resonant distances (mm)
44.60 ± 0.005
43.65 ± 0.005
42.70 ± 0.005
41.75 ± 0.005
40.80 ± 0.005
39.85 ± 0.005
38.90 ± 0.005

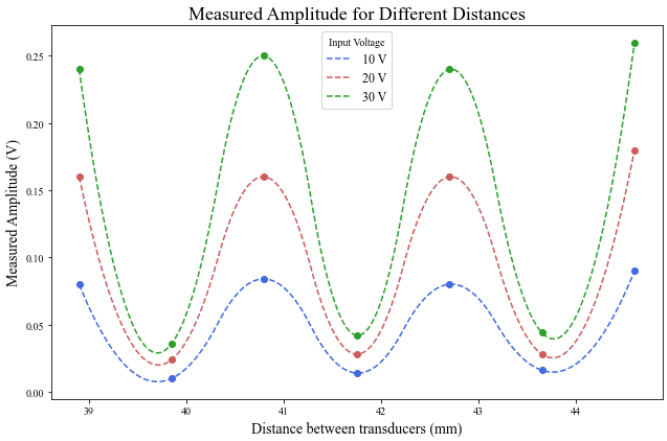

Figure 3.10 - Values of amplitude measured for different distances between transducers, with a spline interpolation.

The initial location of the transducer (44.60 mm) allowed a maximum of amplitude, and a minimum was detected approximately 0.950 mm later. Another maximum was noticed after an additional 0.950 mm displacement. This pattern was consistent until the transducer could no longer be moved.

As mentioned in 1.2.2.4, the theoretical resonant distances (L) between transducers are given by Equation 5. Considering water ($c = 1481\ m/s$) as the main propagation material in this experiment, the wavelength of the acoustic signal is determined by Equation 4:

$$\lambda = \frac{1481}{1.00 \times 10^6} \Leftrightarrow$$

$$\Leftrightarrow \lambda = 1.481\ mm$$

Given this, from Equation 5, the theoretical resonant distances of this setup were determined and are present in Table 3.8.

Table 3.8 - Theoretical resonant distances obtained from Equation 5.

	Theoretical resonant distances (mm)
$L\ (n = 52)$	38.51
$L\ (n = 53)$	39.25
$L\ (n = 54)$	39.99
$L\ (n = 55)$	40.73
$L\ (n = 56)$	41.47
$L\ (n = 57)$	42.21
$L\ (n = 58)$	42.95
$L\ (n = 59)$	43.69
$L\ (n = 60)$	44.43
$L\ (n = 61)$	45.17

Theoretically, a resonant distance should be found every 0.741 mm. Therefore, the experimentally measured distance of 0.950 ± 0.005 mm corresponds to an error of approximately $28.2\% \pm 0.7\%$. This discrepancy arises because the theoretical calculations assume that the ultrasound propagates exclusively through water, which is an approximation. In reality, the wave also travels through the material of the Ibidi slide, which influences its speed and wavelength, and consequently, the observed resonant distances.

Figure 3.9 shows that higher input voltages always promote higher measured amplitudes. However, it is noticeable that discrepancies of maximum amplitudes are more pronounced than discrepancies of minimum amplitudes. Maximum amplitudes result from constructive interference, which amplifies the acoustic wave as the input voltage increases. In contrast, minimum amplitudes are caused by destructive

interference, which ideally cancels out the wave. However, due to reflections and distortion, this cancellation is never total, and as a result amplitudes tend to remain low across different input voltages.

The concept of changing the distance between the transducers while an acoustic standing wave was maintained was found particularly interesting within the scope of this project. If moving a transducer can change the strength of the acoustic field in a specific location, then this movement is also expected to induce spheroids' displacement, which could be a valuable strategy for enhancing alignment. Therefore, this idea was tested with HDF spheroids displaced in an 8-Well Ibidi slide.

First, spheroids were prepared (Section 2.1.2) and 0.300 µl of spheroid suspension was inserted into each of the two vertically aligned central wells of an 8-Well Ibidi slide. The slide was then placed in Setup B, which was carefully filled with water, ensuring it did not reach the lid to avoid contamination. The circuit of the signal generator and amplifier was connected to both transducers and a 1.00 MHz, 30 V signal was applied. Figure 3.11 shows the results of this experiment.

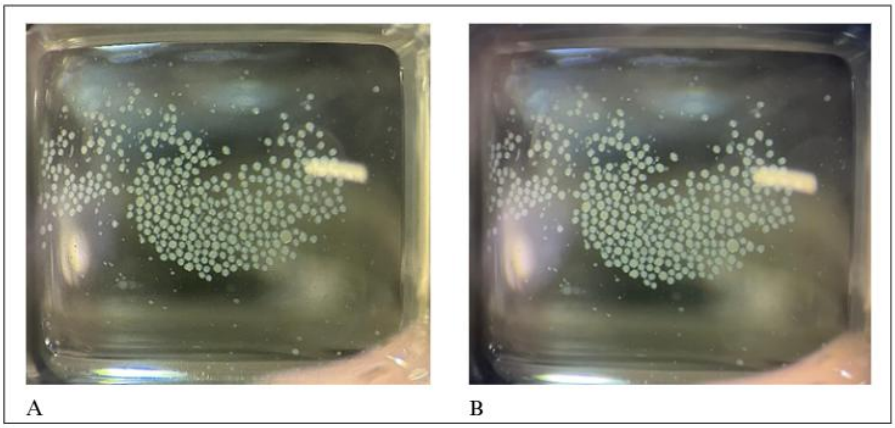

Figure 3.11 - Spheroids in an 8-Well Ibidi chamber slide. A - Before the experiment; B - After the experiment, with the acoustic signal on. Images were taken through the lens of a stereo microscope.

The acoustic signal seemed to have no significant effect on spheroids, since no movement was noted upon activation of the equipment. The input voltage was varied during the experiment to assess whether a stronger signal could promote displacement, but no alignment occurred. Minor movements were observed when the distance between the transducers was changed, but these were insufficient to produce alignment. The only intervention that interestingly seemed to impact spheroids movement was tapping gently on the slide, which indicates that mechanical disturbances could have a positive influence on manipulating them.

This lack of movement of spheroids using Setup B, even under high voltages of 60 V, raised concerns about the efficiency of the PIC181 transducers. Setup A has been used for the same purpose and has proven effective in promoting spheroids displacement. For better understanding, a comparable experiment between these setups was carried out.

3.3.5. Comparison between Transducers

In this experiment, microparticles were used to evaluate alignment, which was assessed by time to align. The input voltage was 30 V, and the frequencies of the signal were 1.66 MHz and 1.00 MHz for

setups A and B, respectively. This experiment was repeated three times for each setup, and the results are presented in Figure 3.12.

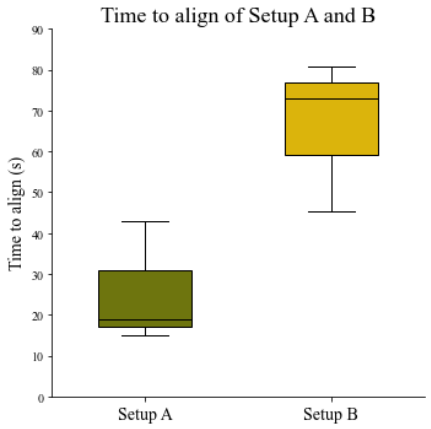

Figure 3.12 - Differences in time to align particles between Setup A and B.

Substantial variability was observed within each setup, suggesting that other factors may have influenced the alignment. The experiments for each setup were conducted under the same conditions, and the only variable that changed was the location of the captured images. As mentioned previously, the adopted method to choose these locations introduces bias into the process, and since alignment is not homogeneous throughout the chamber, this likely contributed to the variability of the results. Increasing the number of samples could potentially improve the reliability of this experiment.

Setup B always exhibited longer alignment times for microparticles than Setup A. This may suggest that PIC181 transducers are less effective than the M165D25 transducers, probably due to the presence of a stainless steel foil in the second ones, which works as a good coupling material. Furthermore, the conditions between setups were not consistent, as the volume of water outside the chamber was not the same. At this time, this factor had not been considered as a potential influence on the acoustic field, though it was identified at later stages as a possible source of variability.

Setup A had been used in previous and concurrent experiments to this project by researchers from the ZMBH. It had shown efficiency in aligning spheroids, but due to its high frequency, the alignment bands created were close to each other. This proximity caused the fusion of spheroids from adjacent bands, disrupting the desired pattern. This limitation motivated the investigation of the PIC181 transducers, which operate at a lower frequency and may produce wider spacing between bands. Additionally, the round shape of the M165D25 transducers limits the area of the acoustic field, while the PIC181 transducers can affect more chambers of the slide.

For these reasons, the PIC181 transducers were not disregarded, despite their longer alignment times. Instead, experiments were conducted to identify the optimal conditions under which they could perform effectively. As part of this process, frequencies that resulted in higher amplitudes within the chamber in Setup B were explored.

3.3.6. Frequency Analysis

In this phase, a frequency sweep was performed using the fourth configuration on Setup B, while maintaining the same value of input voltage. The results of this experiment are presented in Figure 3.13.

For each selected frequency, three amplitude measurements were taken, and the plotted points represent their mean values. The input voltage was 25 V, and no other factor was altered apart from the frequency.

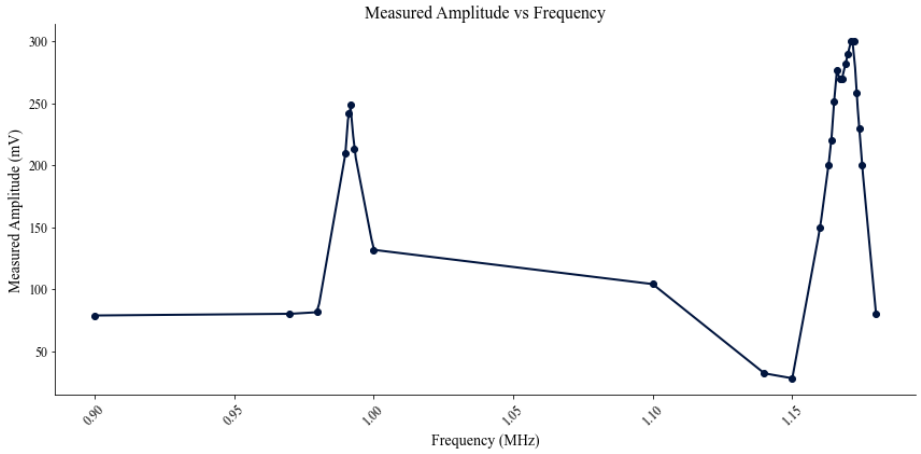

Figure 3.13 - Measured amplitudes in a frequency sweep.

All frequencies between 0.90 MHz and 1.25 MHz were analysed, in steps of 0.01 MHz, to map the overall response profile. However, amplitude was only registered for those frequencies that seemed most relevant. When a certain frequency exhibited an increase in amplitude, additional measurements were carried out around that region with a resolution of 0.001 MHz.

From this analysis, two frequencies were identified as providing maximum of amplitude, therefore being possible resonance points: 0.992 MHz and 1.171 MHz. These frequencies, particularly the second one, are close to the theoretical resonance frequencies of the transducers (0.970 MHz and 1.170 MHz), which were determined previously to this project. To confirm these theoretical values, an impedance analysis of the PIC181 transducers was repeated in this work, yielding resonance frequencies of 0.997 MHz and 1.119 MHz. While the second frequency is very different from the previous results, the first one is close to the experimental resonance of 0.992 MHz. For this reason, the movement of HDF spheroids tested in 3.3.4 was repeated at 0.992 MHz (Figure 3.14).

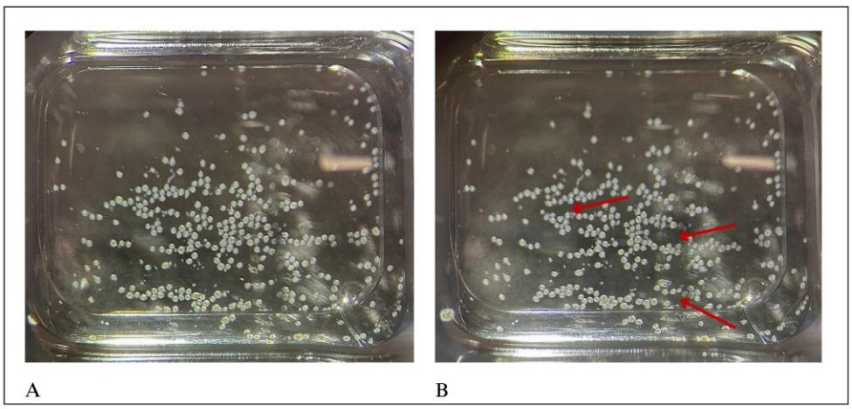

Figure 3.14 - HDF spheroids placed in an 8-Well Ibidi chamber slide. A - Before the experiment; B - After the experiment, with the acoustics on. Red arrows indicate changes in spheroid positions.

Figure 3.14B illustrates the effect of varying the distance between the transducers for an input voltage of 50 V. Under these conditions, spheroids seemed to move to node positions, and gaps between bands were created, even though the overall alignment remained poorly defined. These observations suggest that operating the transducers of Setup B at 0.992 MHz may provide a stronger and more effective acoustic field than at 1.00 MHz. This study also indicates that changing the distance between piezos could be a useful and effective approach to manipulate spheroid positioning and enhance alignment.

3.3.7. Water Volume Analysis

The water levels inside and outside the Ibidi slide were also tested as parameters that could influence the amplitude inside the chamber and consequently the quality of the alignment. Therefore, volumes of water inside two of the chambers of an 8-Well Ibidi slide were varied, as well as the volume of water outside the slide, for Setup B.

In this phase, the amplitude inside the chamber was measured for an internal water volume range of 100 – 300 µl, with steps of 20 µl. For each of these volumes, the volume of water outside the chamber was varied between 30 and 45 ml. This experiment was conducted at 0.992 MHz with an input voltage of 30 V, and the results are illustrated in Figure 3.15.

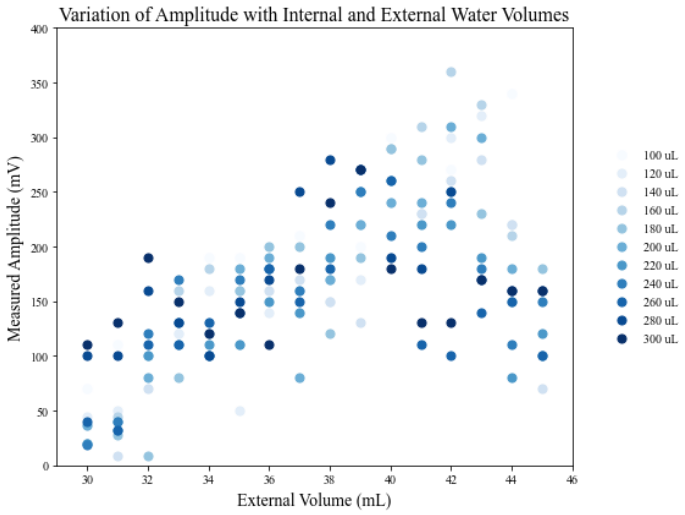

Figure 3.15 - Measured amplitude for different external and internal water volumes, for an input voltage of 30 V.

The results of this experiment showed no consistent pattern in the measured amplitude as water volumes were varied. This indicates that the measured amplitude for a given external volume does not vary in the same way with internal volume as it does for a different external volume. During this experiment, it was observed that the tabs of the Ibidi slide were fully covered only for external volumes greater than 33 ml. When adding water outside the chamber, surface tension effects were noticed, and attempts were made to minimize them by moving the water. The bottom of the well was fully covered for internal volumes equal or greater than 120 µl. Adding water inside the chamber with a transducer placed in it was challenging, as the water tended to adhere to the transducer rather than dispersing

throughout the chamber. These difficulties could have impacted the results, but they were not considered the main cause of the lack of consistent patterning.

Based on these observations, a Python code was developed to understand which combinations of water volumes could provide the best results. Only external and internal volumes equal or greater than 34 ml and 120 µl, respectively, were considered. Then, a threshold was applied to filter amplitudes greater than half the maximum measured amplitude registered in the experiment. Finally, only results with a variation of the amplitude less than 0.15 relative to their neighbours were considered, highlighting regions of local stability to ensure that small changes in water volume do not significantly impact the measured amplitude. The combinations of water volumes which fulfil these requirements are highlighted in dark blue in Figure 3.16.

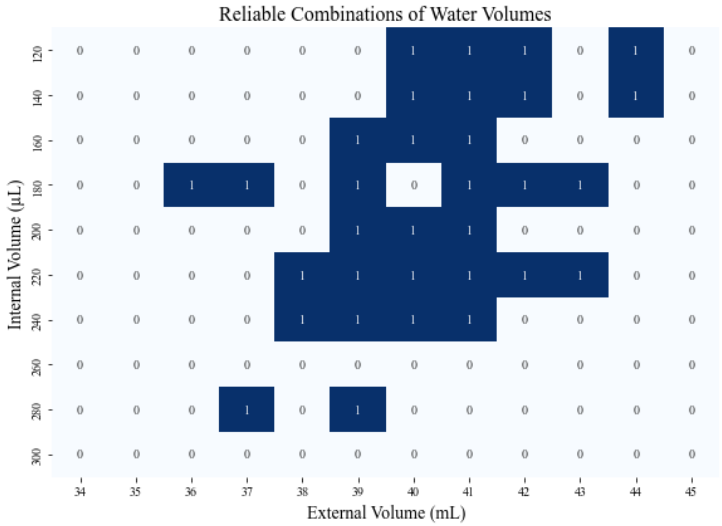

Figure 3.16 - Reliable combinations of internal and external volumes (in dark blue).

This analysis shows the reliable combinations of water volumes, which correspond to operating conditions that are less sensitive to variations in water volume while maintaining a strong response. The biggest reliable zone found was when the internal volume was between 200 and 240 µl and the external volume between 39 and 41 ml. In order to confirm these results and improve the reproducibility of these findings, this experiment was repeated. The same range of internal water volume was tested, but only external volumes greater than 37 ml were considered, since they seemed to be the most relevant. However, while the initial experiment was conducted with an input voltage of 30 V, the repeated experiment was performed with only 20 V by mistake. This error is expected to affect only the absolute amplitude values, and the relative variations should remain unaffected. Therefore, this experiment was still considered valid and relevant for this project. The results of this repetition are shown in Figure 3.17 and Figure 3.18.

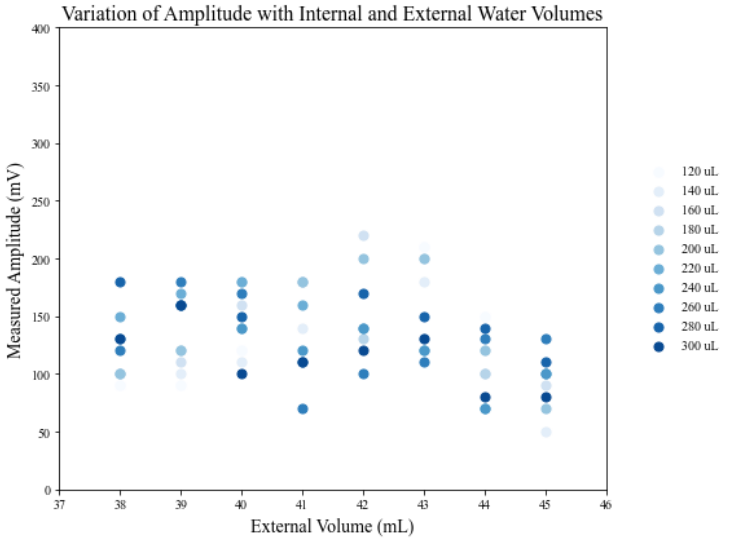

Figure 3.17 - Measured amplitude for different external and internal water volumes, for an input voltage of 20 V.

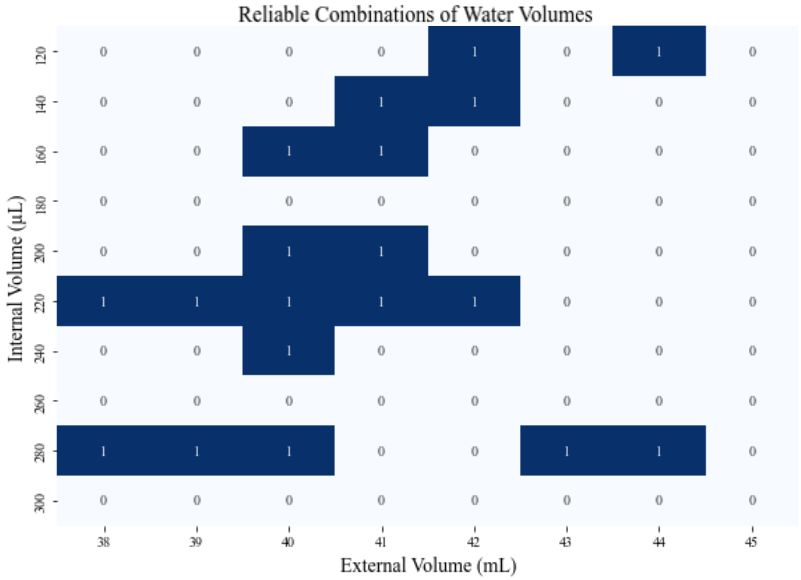

Figure 3.18 - Reliable combinations of water volumes, for an input voltage of 20 V.

Figure 3.17 shows again no consistent pattern in the measured amplitude, which is in accordance with the previous results. However, the reliable combinations of water volumes determined in this experiment differ from those identified earlier. The previously observed reliable zone of 200 – 240 µl of internal volume and 39 – 41 ml of external volume is not observed in this repetition. Instead of 9 reliable combinations in those ranges, only 6 combinations are now visible. Overall, 15 reliable combinations were consistent between experiments, 4 new ones appeared and 14 from the first experiment were not found here. This variation between experiments is unclear, but it might be related to limitations of the experimental setup, since, as mentioned, it was difficult to control and reduce the surface tensions created outside and inside the chamber of the Ibidi slide. These surface tensions may have caused an impact on the distortion of the ultrasound wave, thereby influencing the amplitude measured by the vertical transducer. Therefore, it is not possible to determine with certainty which combinations can be considered reliable. Nevertheless, for further experiments with Setup B, the combination of water volumes used as ideal was 40 ml and 220 µl. This choice was based on three

factors: it was identified as reliable in both experiments; 220 µl was the internal volume that yielded the highest number of consecutive reliable combinations; and 40 ml was the external volume that allowed reliable combinations not only with 220 µl but also with the adjacent internal volumes.

It is relevant to note that the internal and external volumes of water considered in this experiment were particular of an 8-Well Ibidi slide placed on Setup B. For setups and slides with different designs, the ideal volumes would not be the same, as what determines the acoustic behaviour is the water height relative to the chamber. For this reason, Setup B was designed in SolidWorks and an approximation of the water level height outside the chamber (which corresponds to a volume of 40 ml) was determined. The calculated height was approximately 4.05 mm from the bottom of the Ibidi slide.

3.3.8. Final Analysis

Based on insights gained from the conducted experiments, a final study in this phase was performed using Setup B to evaluate how a combination of factors influences spheroids alignment. This experiment assessed the interactive effects of input voltage, frequency, water volume inside the chamber and water volume outside the slide. Spheroids were inserted in an 8-Well Ibidi slide, and their behaviour was captured every 5 seconds on the EVOS microscope. As previously mentioned, the images were captured in a region of the chamber that was initially assessed and considered as the location that provided better results.

The parameters tested are present in Table 3.9 and 16 experiments were conducted.

Table 3.9 - Values of factors tested.

Factor	**Low level**	**High level**
Input Voltage (V)	30.0	50.0
Frequency (MHz)	0.992	1.171
Volume of water inside the chamber (µl)	180	220
Volume of water outside the chamber (ml)	40.0	45.0

The input voltage levels (30.0 and 50.0 V) were chosen considering previous experiments, which showed that this range is optimal to ensure spheroid movement. The frequencies tested correspond to the experimentally determined resonance frequencies from the frequency sweep (Section 3.3.5), in order to confirm which one yields the best performance. Regarding the water volumes, 220 µl and 40.0 ml were chosen, as they had previously provided the highest number of reliable combinations, whereas 180 µl and 45.0 ml were included as contrasting conditions, since they were associated with no reliable combinations in the last experiment. This choice of volumes was intended to confirm the amplitude results obtained in the previous analysis.

The movement of the spheroids was analysed by their mean net displacement and mean speed, which were obtained from the MATLAB script. The results are presented in Figure 3.19.

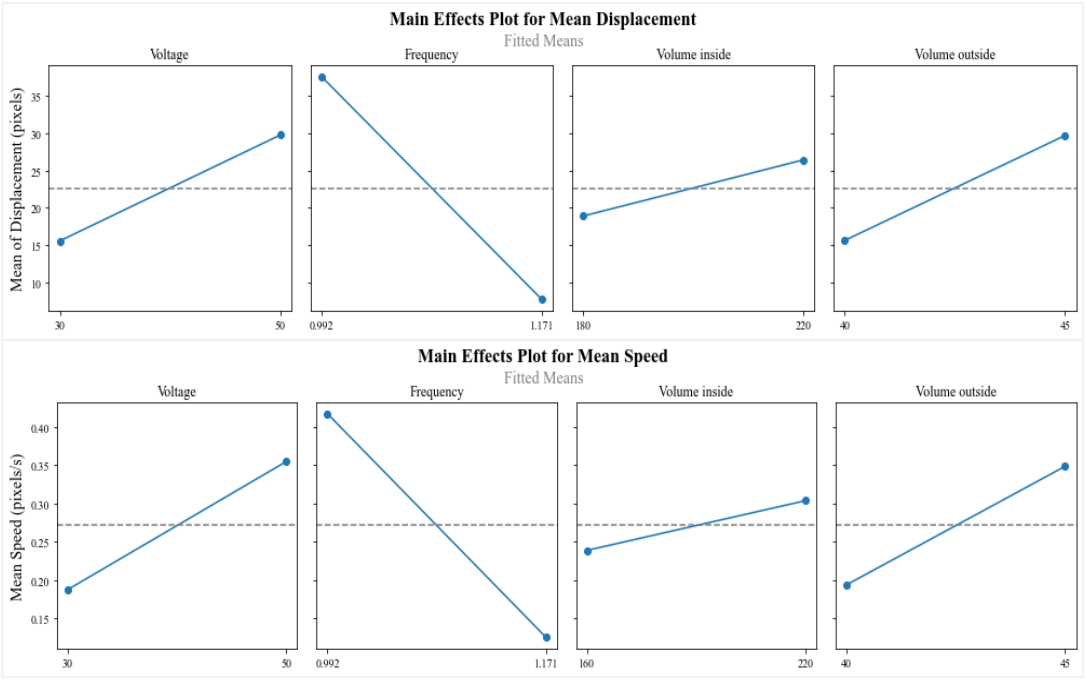

Figure 3.19 - Main effects of factors on mean displacement and mean speed of spheroids.

Mean displacement and mean speed exhibited similar behaviours in terms of how factors influenced them, indicating that conditions which increased the displacement of the spheroids also increased their speed, and vice-versa. This experiment showed that 50.0 V allowed a faster and longer spheroid movement compared with 30.0 V. Frequency appeared to have the most impact on spheroid movement, as 1.171 MHz did not create an acoustic field sufficient to shift the spheroids, whereas 0.992 MHz did, confirming the effectiveness of applying a 0.992 MHz signal. As expected, 220 µl of water inside the chamber yielded a better performance than 180 µl. Finally, opposite to what was expected, 45.0 ml of water outside the chamber allowed a higher displacement and a faster movement of the spheroids than 40.0 ml. This contradicts both analyses conducted in the previous section, which may be due to several factors, including errors in volume measurement and dispensing, the presence of outliers (e.g. regions with more movement while in other regions spheroids remained static), and acoustic streaming effects caused by high voltages, which might influence spheroid displacement. In order to confirm these findings, more experiments would be necessary.

The interaction plots for both responses are present in Figure 3.20.

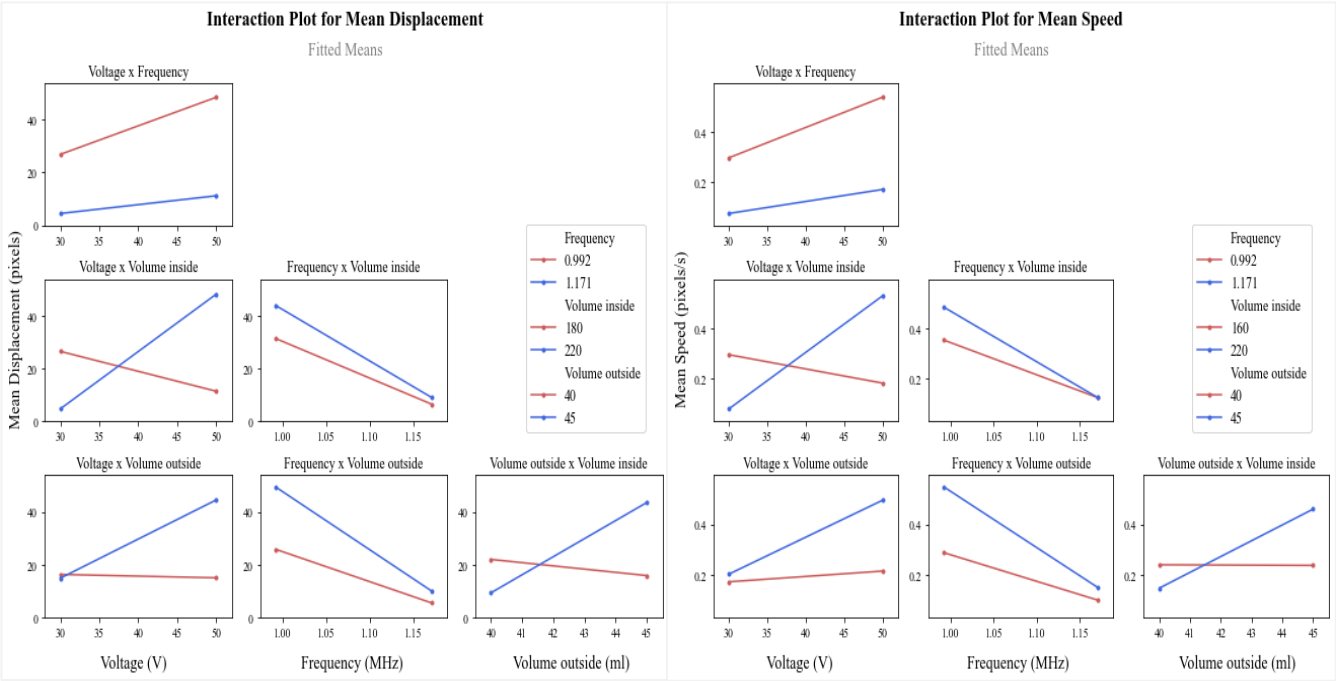

Figure 3.20 - Interactions between factors for mean displacement (left) and mean speed (right).

These plots show similar trends between mean displacement and mean speed, confirming their equal behaviours. All factors seem to interact with each other, since none of the plots show parallel lines. However, some interactions are stronger than others. For example, voltage appears to interact more strongly with the internal water volume than with the frequency. This means that the effect of voltage on spheroid movement depends more on the internal water volume than on the frequency.

To better understand the effects of these factors on both responses, a Pareto Chart of the Effects was determined for each one using Lenth's method (Figure 3.21).

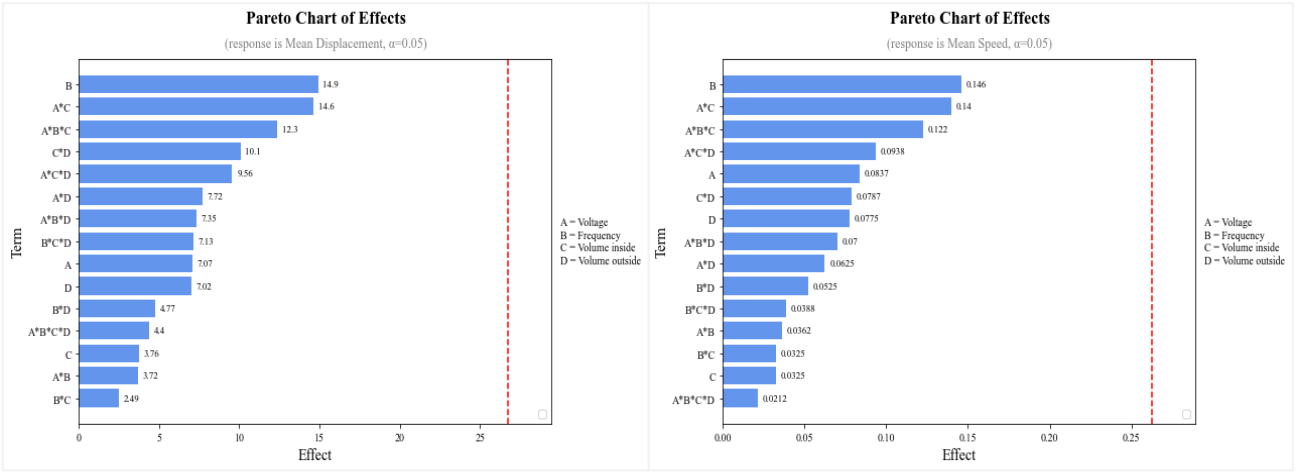

Figure 3.21 - Pareto chart of effects for mean displacement (left) and mean speed (right).

There are no factors or combinations of factors that significantly impact the mean displacement and mean speed of the spheroids. However, frequency is the factor that has a greater impact on these responses, followed by the interaction between voltage and the volume inside the chamber.

Mean displacement and mean speed are quantitative measures of spheroid movement, but they do not indicate or quantify the alignment itself. As mentioned previously, time to align and wave distortion were relevant to analyse the alignment of particles, but they could not be used for spheroids, unlike what was initially thought, because the Voronoï method developed in ImageJ was not optimized to detect larger structures than microparticles. Therefore, other methods and measures to quantify spheroid alignment are necessary, but they were not developed within the scope of this work, due to time constraints. Instead, the alignment in these experiments was visually assessed and although displacement was noticed, spheroids did not organise in bands, and alignment was either non-existent or very poorly defined. This might be explained by the size and weight of the HDF spheroids, which are significantly larger and heavier than microparticles. Therefore, the ARF applied to these spheroids must be strong enough to counter the adhesion forces to the bottom surface and push the spheroids to node positions.

It is also important to mention that, since no alignment was reached and trajectories were often irregular, the total path travelled, although determined by the MATLAB script, was not considered an informative metric. Instead, the mean net displacement between initial and final positions was used, as it provides a more reliable measure of the overall effect of the acoustic field on spheroid movement.

3.3.9. Quality Function Deployment

The analysis performed until this stage allowed a better understanding of the factors that influence the alignment of spheroids with standing waves. Therefore, in this phase, all conditions were met for the final development of the QFD. The first matrix is presented in Figure 3.22.

Legend		
⊙	Strong Relationship	9
○	Moderate Relationship	3
▲	Weak Relationship	1
++	Strong Positive Correlation	
+	Positive Correlation	
−	Negative Correlation	
▼	Strong Negative Correlation	
▼	Objective Is To Minimize	
▲	Objective Is To Maximize	
x	Objective Is To Hit Target	

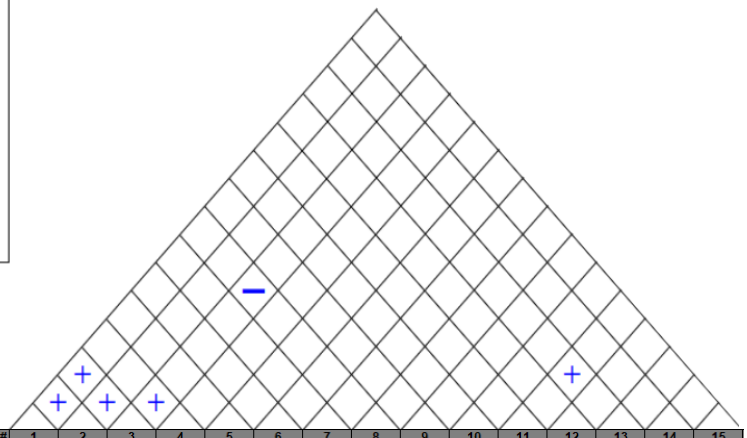

Row #	Max Relationship Value in Row	Relative Weight	Weight / Importance	Demanded Quality (a.k.a. "Customer Requirements" or "Whats") \ Quality Characteristics (a.k.a. "Functional Requirements" or "Hows")	1 Initial amplitude of wave (V)	2 Frequency (MHz)	3 Amplitude after propagation (V)	4 Increase of spheroids in ROI (%)	5 Wave distortion (um)	6 Direction of alignment (°)	7 Deviation from initial alignment after disturbance (um)	8 Time to align (s)	9 Thermal stability	10 Ethanol resistance	11 Dimensions (mm)	12 Shape	13 Weight (g)	14 Structural rigidity	15 Light Transmittance (%T)
				Column #	1	2	3	4	5	6	7	8	9	10	11	12	13	14	15
				Direction of Improvement: Minimize (▼), Maximize (▲), or Target (x)	x	x	▲	▲	▼	x	▼	▼	▲	▲	x	x	x	▲	▲
1	9	10,8	9,0	Effective signal emission	⊙	⊙													
2	9	12,0	10,0	Efficient acoustic wave propagation		○	⊙	○	○	○		○							
3	9	8,4	7,0	Fast alignment		○	○					⊙							
4	9	12,0	10,0	Precise and robust alignment		○	○	⊙	⊙	⊙	⊙								
5	9	10,8	9,0	Sterilizable									⊙	⊙					
6	9	9,6	8,0	Ease of use inside of hood											⊙	⊙			
7	9	9,6	8,0	Portable without alignment loss							⊙				⊙		⊙		
8	9	8,4	7,0	Mechanical robustness							○					⊙		⊙	
9	9	8,4	7,0	Compatible with imaging techniques												⊙			⊙
10	9	9,6	8,0	Can be placed in the incubator									⊙		○				
				Target or Limit Value	Equal to voltage generated by the circuit	0.992 MHz	Equal to initial voltage	100%	0 um	Parallel to transducers	0 um	Minimum	No loss of properties after test	No loss of properties after test	-	-	-	No loss of properties after test	100%
				Difficulty (0=Easy to Accomplish, 10=Extremely Difficult)	6	3	8	9	9	7	8	7	6	6	4	2	2	6	3
				Max Relationship Value in Column	9	9	9	9	9	9	9	9	9	9	9	9	9	9	9
				Weight / Importance	97,6	195,2	169,9	144,6	144,6	144,6	220,5	112,0	184,3	97,6	202,4	238,6	86,7	75,9	75,9
				Relative Weight	4,5	8,9	7,8	6,6	6,6	6,6	10,1	5,1	8,4	4,5	9,2	10,9	4,0	3,5	3,5

Figure 3.22 - First matrix of House of Quality.

The quality drivers established in 3.2. were weighted given their importance. “Efficient acoustic wave propagation” and “Precise and robust alignment” were considered the most relevant, as the main goal is to have a strong acoustic field capable of aligning spheroids in a controlled pattern. “Effective signal emission” and “Sterilizable” were weighted with an importance of 9/10, since to have a strong acoustic field is very important to have an effective signal emission, and in this context of tissue engineering, it is crucial that the environment where spheroids are placed is sterile, allowing for their safe growing and tissue development. “Ease of use inside of hood”, “Portable without alignment loss” and “Can be placed in the incubator” were ranked next in importance. To ensure sterility, experiments

with biological materials should be performed inside a hood, therefore it is relevant that the setup can be easily handled in this environment. The spheroids will need to be transported during and/or after the experiment, so it is important these movements do not prejudice the resulting alignment. After the experiment, spheroids should be placed inside an incubator, which allows the proper conditions for their development. Finally, "Fast alignment", "Mechanical robustness" and "Compatible with imaging techniques" were weighted with an importance of 7/10. These remain relevant but were considered less critical.

Each CTQ was assigned with a target value, and a difficulty level to achieve it. The initial amplitude of the wave should be equal to the voltage generated by the system, without losses of energy. The frequency should be the resonant frequency of the transducers, which was discovered to be 0.992 MHz for the PIC181. An optimal amplitude of the wave after propagation is equal to the initial voltage, which is difficult to accomplish, as the wave tends to lose energy as it travels. The increase of spheroids in a ROI should be 100% and wave distortion should be minimal, in order to have a precise alignment, even though this was discovered as a difficult task. The direction of alignment of the spheroids should be oriented by node positions, therefore parallel to the transducers position, but due to factors that disturb the acoustic field, this is also difficult to accomplish. The deviation from initial alignment after disturbance and the time to align should be minimized, but again this is also challenging. The thermal stability, ethanol resistance and structural rigidity can be evaluated through tests and are optimal when no properties are lost. The light transmittance of the setup should be maximized to allow visualization of the results. The dimensions, shape and weight of the setup were not assigned with target values, as at this stage of the project it was not possible to conclude optimal targets for these CTQs.

Certain CTQs are correlated with each other, as proven by experiments conducted in this project. A resonant frequency allows an increase in amplitude of the wave, and the greater the initial amplitude, the greater the amplitude after propagation. An increase in this amplitude promotes an increase in spheroid movement, thereby influencing the number of spheroids in a ROI and the time required for them to align. Finally, the bigger the setup, the heavier it becomes.

Relationships were established between quality drivers and CTQs. An "Effective signal emission" can be assessed by the initial amplitude of the wave and the frequency of the signal. The amplitude of the wave after propagation is a direct indicator of "Efficient acoustic wave propagation". The frequency of the signal was proven to influence the amplitude of the wave, thereby affecting its propagation. The increase of spheroids in a ROI, the wave distortion, the direction of alignment and the time to align are indirect indicators of the same driver, as they assess the quality of alignment which depends on an efficient wave propagation.

A "Fast alignment" is assessed by time to align and depends on the amplitude of the wave after propagation and on the frequency of the signal. On the other hand, a "Precise and robust alignment" is directly assessed by the increase of spheroids in a ROI, wave distortion, direction of alignment and deviation from initial alignment after disturbance. To achieve this, the frequency of the signal should be optimal, as well as the amplitude after propagation.

A "Sterilizable" setup is a setup that can be autoclaved and ethanol sterilized, and therefore is assessed by the thermal stability and ethanol resistance of its components. "Ease of use inside of hood" is a requirement that depends only on the dimensions and shape of the system.

A setup "Portable without alignment loss" can be assessed by the deviation from initial alignment after disturbance and depends on its shape and weight. The "Mechanical Robustness" should be

evaluated based on the structural rigidity of the setup and its shape, which will affect the deviation from initial alignment, as well.

To be “Compatible with imaging techniques” it should have an optimized shape and a high value of light transmittance. Finally, a setup that “Can be placed in the incubator” needs to be thermally stable and have suitable dimensions.

The first matrix of the QFD usually also allows to perform a competitive analysis, in order to compare the concept to other alternatives already in the market. This was not considered to be within the scope of this work, as the main goal was only to develop a design concept based on experimental analysis. The translation of this design into a final product was not accomplished but might be relevant to consider in a future perspective.

The second matrix was completed, as shown in Figure 3.23. In this matrix, product features were assigned to each CTQ.

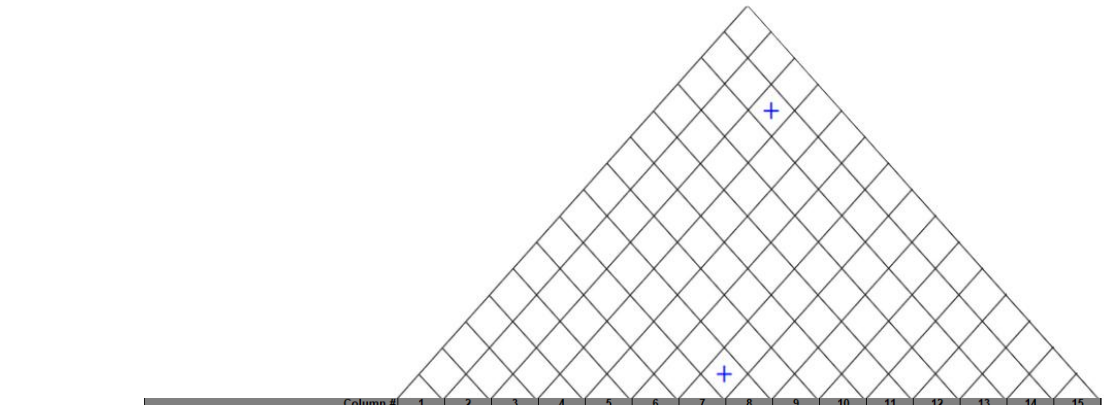

Row #	Max Relationship Value in Row	Relative Weight	Weight / Importance	Demanded Quality (a.k.a. "Customer Requirements" or "Whats")	Electrical conductivity	Transducer sensitivity	Acoustic Impedance Mismatches (rayl)	Acoustic Attenuation coefficientes (dB/m)	Concentration of spheroids (number/mm^3)	Radius of spheroids (um)	Angle of incidence of wave on material (°)	Transducers position	Distance between transducers (mm)	Dimensions of chamber for spheroids (mm)	Working temperature of transducers (°C)	Operating temperature range (°C)	Surface area exposed to ethanol (mm^2)	Density of materials (g/cm^3)	Bottom transparency
				Column #	1	2	3	4	5	6	7	8	9	10	11	12	13	14	15
				Direction of Improvement: Minimize (▼), Maximize (▲), or Target (x)	▲	▲	▼	▼	x	x	x	x	x	x	▼	▲	▼	x	▲
1	9	4,5	97,6	Initial amplitude of wave (V)	⊙	⊙													
2	9	8,9	195,2	Frequency (MHz)		⊙													
3	9	7,8	169,9	Amplitude after propagation (V)			⊙	⊙					○					○	
4	9	6,6	144,6	Increase of spheroids in ROI (%)			⊙	⊙	⊙	⊙	⊙	⊙	⊙	⊙				○	
5	9	6,6	144,6	Wave distortion (um)					▲	⊙	⊙	⊙							
6	9	6,6	144,6	Direction of alignment (°)						○	⊙	⊙							
7	9	10,1	220,5	Deviation from initial alignment after disturbance (um)					▲	⊙									
8	9	5,1	112,0	Time to align (s)			⊙	⊙	⊙	⊙			○	○				○	
9	9	8,4	184,3	Thermal stability											⊙	⊙			
10	9	4,5	97,6	Ethanol resistance													⊙		
11	9	9,2	202,4	Dimensions (mm)									⊙	⊙					
12	9	10,9	238,6	Shape								⊙	○						⊙
13	9	4,0	86,7	Weight (g)														⊙	
14	9	3,5	75,9	Structural rigidity														⊙	
15	9	3,5	75,9	Light Transmittance (%T)															⊙
				Target or Limit Value	Maximum	Maximum	0	0	-	1000um	0	Horizontal	Resonant distance	-	< 40°C	20 - 40°C	Minimum	-	Maximum
				Difficulty (0=Easy to Accomplish, 10=Extremely Difficult)	4	5	9	9	6	2	7	7	6	6	4	6	6	4	2
				Max Relationship Value in Column	9	9	9	9	9	9	9	9	9	9	9	9	9	9	9
				Weight / Importance	40,1	120,3	175,2	175,2	122,1	275,2	178,2	276,2	213,9	157,9	75,7	75,7	40,1	125,2	129,2
				Relative Weight	1,8	5,5	8,0	8,0	5,6	12,6	8,2	12,7	9,8	7,2	3,5	3,5	1,8	5,7	5,9

Figure 3.23 - Second matrix of House of Quality.

The initial amplitude of the wave depends strongly on the electrical conductivity of the components and on the sensitivity of the transducer on converting an electrical signal into an ultrasound. The frequency also depends on this sensitivity and the amplitude after propagation is directly affected by acoustic impedance mismatches between materials and their acoustic attenuation coefficients. For this reason, the density of the materials has an indirect effect on this CTQ, as well as the distance between transducers, which was proven in Section 3.3.3. to have an impact on the amplitude of the wave.

The number of spheroids in a ROI depends on many features: acoustic impedance mismatches and attenuation coefficients, concentration of spheroids and their radius, the angle of incidence of the wave

on the material, the transducer's position and the distance between them, the dimensions of the chamber, and indirectly, the density of the materials. Wave distortion, a measure of irregularities in the acoustic field, is controlled by the acoustic impedance mismatches and the angle of incidence of the wave on materials. On the other hand, the direction of alignment, which measures the alignment shift, is affected by the transducer's position and the angle of incidence of the wave on the materials. After a disturbance, the deviation from initial alignment depends on the structural rigidity of the setup, therefore depending on the density of its materials. It also depends on the radius and concentration of spheroids, as larger spheroids require more intense disturbances to move, and the forces acting between them also influence their movement. Time to align is affected by material properties, such as acoustic impedance, attenuation coefficients and density, and by the concentration of spheroids and their radius. It is also expected to be influenced by the distance between transducers and the dimensions of the chamber.

The thermal stability can be affected by the temperature of the transducers during their operation and the environmental temperature. The ethanol resistance depends on the surface area of the setup that must be exposed to ethanol during sterilization. The distance between transducers and the dimensions of the chamber dictate the overall dimensions of the setup, while its shape is defined by the bottom transparency, the order of discontinuities, and therefore the impedance mismatches, the transducer's position and the distance between them, as well as the surface area exposed to ethanol. The weight of the setup and its structural rigidity depend on the density of the materials, and the light transmittance on the transparency of the bottom.

Each of these product features was assigned with a target value and a difficulty in accomplishing it. The electrical conductivity and the transducer sensitivity should be maximized, while the acoustic impedance mismatches and the attenuation coefficients should be minimized, which is very difficult to achieve. The spheroids used in this project had a radius of 1000 μm and therefore that was defined as the target value. The angle of incidence of the wave should be null to avoid refractions, and the transducer's position must be completely horizontal to guarantee that. The distance between the transducers must be a resonant distance to maximize the energy of the acoustic field. The temperature of the transducers should not exceed 40ºC, as the maximum temperature of the environment should also be 40ºC (inside an incubator). The surface area exposed to ethanol must be minimized and the bottom transparency maximized to allow visualization of results. No target value was assigned to the concentration of spheroids, the dimensions of the chamber and the density of materials, as in the scope of this project, optimal values for these features were not concluded and further experiments would be necessary.

Finally, a positive correlation was established between the transducer's position and the angle of incidence of the wave, and between the acoustic impedance mismatches and the density of the materials (since $Z = pc$).

3.3.10. Design Concepts

The analysis performed until this stage provided valuable insights about how different factors influence spheroid behaviour under an acoustic field. The analysis conducted in 3.3.1 concluded that the acoustic refractive index was the only factor that significantly influenced the alignment time of the particles, proving that water is a more suitable propagation medium than ultrasound gel. Then, multiple factors and their influence on the acoustic field were investigated based on amplitude measurements. To

prioritize the most critical design characteristics, the maximum variation of the measured amplitude was determined for each factor, and the results are presented in Figure 3.24.

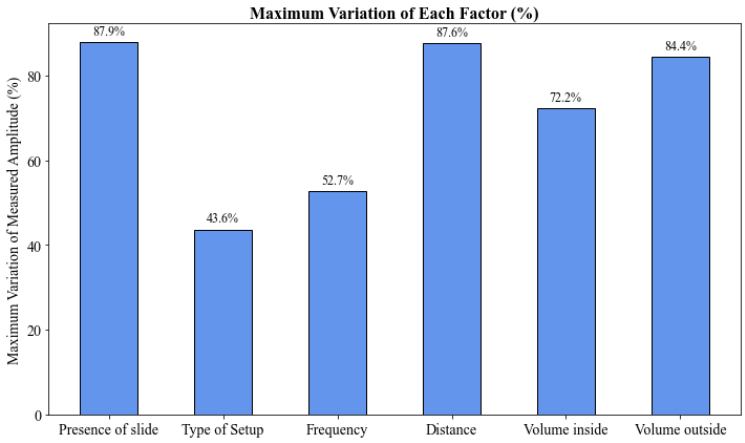

Figure 3.24 - Maximum variation in amplitude obtained of each factor.

These results show that the measured amplitude had a maximum decrease of 87.9% after adding an Ibidi slide to the setup. This indicates that the acoustic field is weakened in the presence of a slide and suggests that spheroid alignment could potentially improve if spheroids were not placed inside a chamber slide. Changing the distance between transducers also led to large changes in amplitude between resonant distances, underlining the importance of placing the transducers at a specific distance to improve the strength of the ARF. Furthermore, the water volume outside the chamber also showed a variation in amplitude greater than 80.0%, demonstrating the relevance of this parameter.

Additional experiments conducted with spheroids, as those described in 3.3.4. and 3.3.8., revealed other important observations. The adhesion forces to the bottom surface of the slide seemed to be stronger than the ARF, impairing the movement and alignment of the spheroids. As mentioned previously, mechanical taps on the slide helped move these structures, by facilitating their detachment.

Based on this information, and considering the customer requirements established in 3.2, different design concepts and alternatives to improve the alignment were studied. First, in order to solve or attenuate the adhesion to the bottom, two possible materials were considered: agarose and an Anti-Adherence Rinsing Solution (STEMCELL Technologies). Agarose is a biomaterial commonly used to modify surfaces, making them non-adhesive. It is a low-cost material, compatible with autoclave sterilization, and often used to avoid cell adhesion to the surface during spheroid generation [34]. The Anti-Adherence Rinsing Solution is a surfactant solution for pre-treating cultureware that reduces surface tension and prevents cell adhesion [35]. Both options were thought to be applied to the bottom surface of a chamber of an 8-Well Ibidi slide. Additionally, it was also thought that wider chambers could potentially reduce surface tension, and therefore 4-Well Ibidi slides were considered as well. To hold these slides, different setups were conceptually designed.

As mentioned, the setup should have a resonant distance between transducers to promote a stronger acoustic field. Nevertheless, it was also shown that changing the distance while the acoustics are on may positively impact the manipulation and alignment of the spheroids. Moreover, the water volume outside the chamber slide should be controlled, as this factor can have a great effect on the amplitude of the acoustic waves. As concluded previously, the presence of a slide between the transducers reduces the amplitude of the acoustic waves, thereby weakening the signal. For this reason, an alternative setup without a chamber slide was also considered.

All design concepts idealized at this stage are described in Table 3.10.

Table 3.10 - Design concepts and their characteristics.

	Setup B (Baseline)	**Concept 1**	**Concept 2**	**Concept 3**
Support material	3D printed epoxy resin	3D printed epoxy resin	3D printed epoxy resin	3D printed epoxy resin
Bottom material	Glass	Glass	Glass	Glass
Support for transducers	Fixed, glued to the front of the transducers	Fixed, glued to the back of the transducers	Movable, glued to the back of the transducers	Fixed, glued to the back of the transducers
Propagation material	Water	Water	Water	HDF spheroid medium
Type of chamber for spheroids	8-Well Ibidi chamber	8-Well or 4-Well Ibidi chamber with a bottom layer of Agarose or Anti-Adherence Rinsing Solution	8-Well or 4-Well Ibidi chamber with a bottom layer of Agarose or Anti-Adherence Rinsing Solution	Open chamber. Medium and spheroids in direct contact with glass bottom and transducers
Overflow chamber	None	Present	Present	None

TRIZ was a useful ideation tool at this stage, as it helped the process of thinking and creating different designs. TRIZ offers 40 inventive principles for solving technical contradictions. For example, in this context, the setup should be stable and robust with fixed components, but that limits the possibility of optimizing alignment conditions. This contradiction was identified as the trade-off between stability and adaptability, and one of the inventive principles proposed by TRIZ to address this issue was "Parameter Change". This principle highlights that performance can be improved by varying parameters in a controllable way, which in this context could be varying the distance between the transducers, rather than fixing them. Another principle proposed by TRIZ was "Separation", which suggested separating interfering components, which was applied by isolating the transducer supports from the slide support, allowing the transducers to be repositioned without disturbing the spheroids. These ideas guided the generation of design concepts, until idealizing the final Concept 2.

The design concepts were then compared and evaluated based on the Pugh Matrix method, as shown in Table 3.11.

Table 3.11 - Pugh Matrix of Design Concepts.

Criteria	**Importance**	**Setup B (Baseline)**	**Concept 1**	**Concept 2**	**Concept 3**
Effective signal emission	9.0	0	0	0	0
Efficient acoustic wave propagation	10	0	1	1	1
Fast alignment	7.0	0	1	1	1
Precise and robust alignment	10	0	1	1	1
Sterilizable	9.0	0	0	0	-1
Ease of use inside of hood	8.0	0	0	0	0
Portable without alignment loss	8.0	0	0	0	-1
Mechanical robustness	7.0	0	0	0	0
Compatible with imaging techniques	7.0	0	0	0	0
Can be placed in the incubator	8.0	0	0	0	-1
Total weighted score		0	27	27	2

The transducers in Setup B are glued to the back of the resin supports and to the petri dish holder (see Figure 2.8). This configuration may cause some ultrasound energy to propagate through the resin and interfere with the bottom surface of the slide, disrupting node positions and consequently the spheroid alignment. Consequently, all three design concepts are expected to improve acoustic wave propagation compared to the baseline, as no material is placed in front of the transducers.

The Ibidi slides with a modified bottom surface, either with Agarose or with the Anti-Adherence Rinsing Solution, are expected to improve spheroid movement, thereby making the alignment faster and more precise. In contrast, Concept 3 does not need an Ibidi slide and spheroids are placed directly on the glass. As mentioned before, this potentially increases the strength of the acoustic field, also making the alignment faster and more precise. However, this design concept is much more difficult to sterilize, as it is necessary to sterilize the whole setup, and transducers are not autoclavable. Additionally, this setup is not advised to be placed in the incubator, as the environment inside it should be sterile. For Concepts 1 and 2, the spheroids can be transported by carefully moving the slide, but for Concept 3, the whole setup needs to be transported, which is more difficult to perform without losing the alignment.

This Pugh Matrix only takes into account the differences between the design concept and the baseline, making no comparison between design concepts. For this reason, Concept 1 and Concept 2 have the same final weighted score, but Concept 2 is expected to provide a more precise alignment than Concept 1, as it allows for changing the distance between transducers. However, its design is more complex, and its fabrication would take longer, as loose components should be carefully minimized to avoid unwanted vibrations.

Despite its low score, Concept 3 was considered intriguing, as it avoids the limitations imposed by chamber slides. For this reason, a prototype of this concept was designed for further testing.

3.4. Design Phase

3.4.1. Prototypes

Concept 3 was designed in SolidWorks, as shown in Figure 3.25, with a resonant distance of 35.06 mm, obtained from Equation 5 for a frequency of 0.992 MHz. It was 3D printed by Stereolithography (SLA) in epoxy resin, and it was then cured and cleaned with isopropyl alcohol. Two PIC181 transducers were glued to its sides. Then, the whole setup was glued and sealed with silicone to a large petri dish. The petri dish was used as an external chamber where water was poured to cool the transducers. This was a preliminary prototype, as the goal was to use glass instead. Figure 3.26 shows the final result.

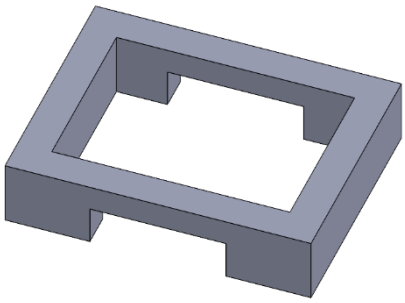

Figure 3.25 - CAD of Concept 3.

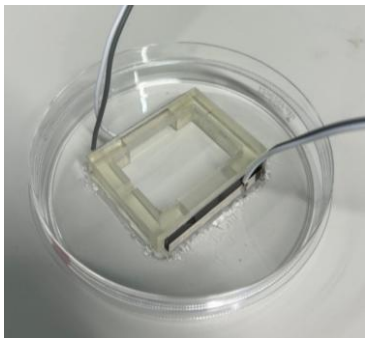

Figure 3.26 - Final prototype of Concept 3, glued to a petri dish.

Concepts 1 and 2 were also designed in SolidWorks (Figure 3.27 and Figure 3.28). Due to time limitations of this project, these prototypes were not printed and remained as conceptual models. Nevertheless, the different types of Ibidi slides proposed as alternatives to the standard 8-Well were studied and their performance was evaluated with spheroids using Setup B.

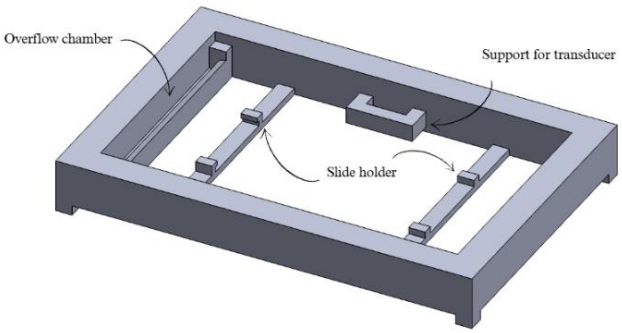

Figure 3.27 - CAD of Concept 1.

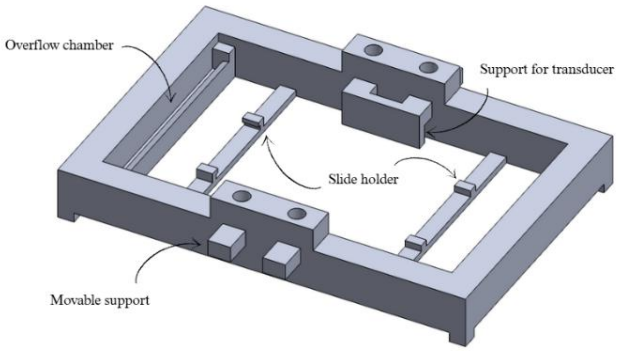

Figure 3.28 - CAD of Concept 2.

3.4.2. Complementary Experiments

To understand the performance of Concept 3 and the efficacy of the slide alternatives, complementary experiments were conducted at this stage. Thus, Setup B was tested with four different chamber slides: 8-Well Ibidi with Agarose; 8-Well Ibidi with Anti-Adherence Solution; 4-Well Ibidi with Agarose; and 4-Well Ibidi with Anti-Adherence Solution.

For the 8-Well slides, 220 µl of spheroid suspension was placed inside a chamber, while for the 4-Well slides 440 µl was used. For Concept 3, as the chamber is wider, it was used 600 µl of spheroid suspension. The external water volume for experiments with Setup B was 40 ml, and for all configurations the input voltage was varied between 20 and 50 V, with steps of 10 V.

Therefore, 20 experiments were conducted, and images were captured every 5 seconds with the EVOS microscope, following the previously described criterion for choosing a chamber location. However, these metrics could not be determined for Concept 3, as the setup vibrated during the experiment and all captured images were blurred, as shown by Figure 3.29.

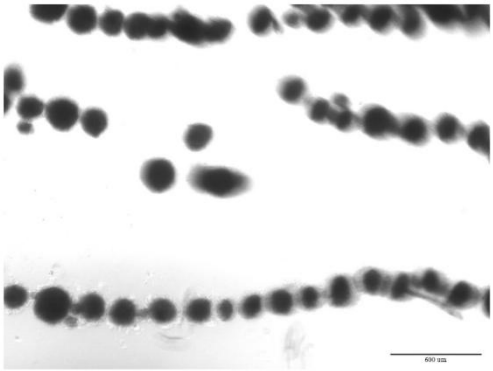

Figure 3.29 - EVOS image captured during experiments with Design Concept 3.

The vibrations intensified with the increase of voltage and therefore only 20 and 30 V were tested under the EVOS. These vibrations might be explained by the movement of the transducers, which were directly glued on the surface where spheroids were placed. Even though it was not possible to measure spheroid movement with this setup, it was observed that alignment occurred within less than 5 seconds (for both voltages), and defined bands were visible.

The results of the remaining experiments are presented in Figure 3.30. To compare the differences between having or not a coat of agarose and anti-adherence solution, the previous results from 3.3.8. related to an 8-Well Ibidi slide for input voltages of 30 V and 50 V were also represented.

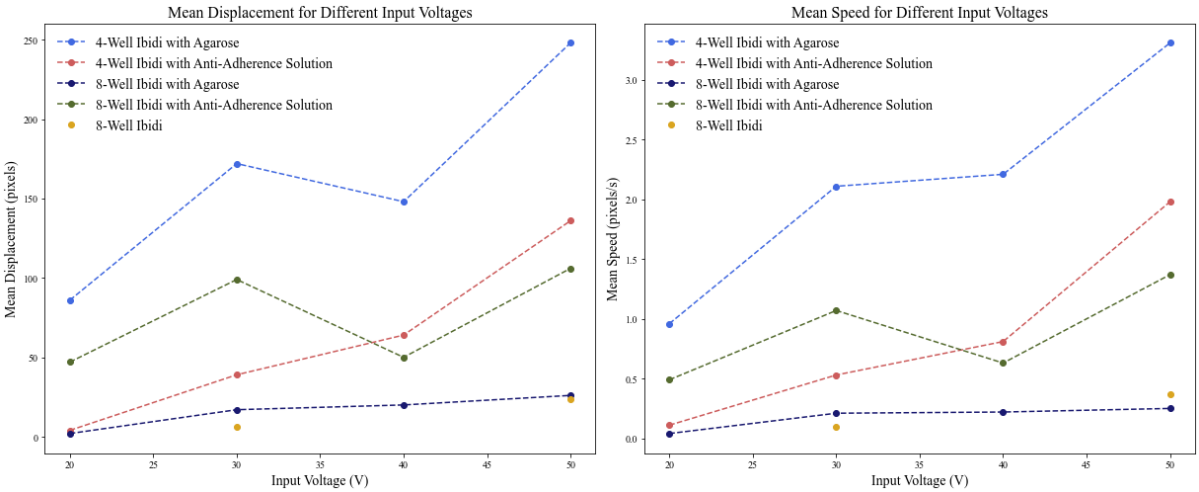

Figure 3.30 - Mean displacement (left) and mean average speed (right) of spheroids for different input voltages and chambers.

The 4-Well with Agarose exhibited the highest mean displacement and speed for all input voltages. However, it exhibited a decrease in displacement between 30 V and 40 V, which was not expected, but may be justified by the chosen region to capture images. Although this region was initially assessed as the one that provided the best results, it does not guarantee consistency, as the number of spheroids in it may vary between experiments.

The 8-Well with Anti-Adherence Rinsing Solution also showed a decrease in both displacement and average speed between the same voltages. After this decrease, its results were lower than the 4-Well with the same solution. The 8-Well with Agarose was the slide that exhibited the worst results for all four experiments, with minor differences between them.

All four configurations exhibited better results in terms of mean displacement than the regular 8-Well Ibidi. This potentially indicates that both the Anti-Adherence Solution and the Agarose promote spheroid movement. However, the differences between having or not an Agarose layer in an 8-Well are very small and inconclusive when analysing the mean speed. This experiment was conducted only once for each configuration and therefore no statistical analysis was performed, as it would not be reliable. To confirm these results and their significance, more experiments are needed.

As before, alignment was not measured, but only visually assessed. For most configurations, only an input voltage of 50 V was enough to promote the organization of spheroids in bands. Figure 3.31 shows the results of each chamber for this voltage.

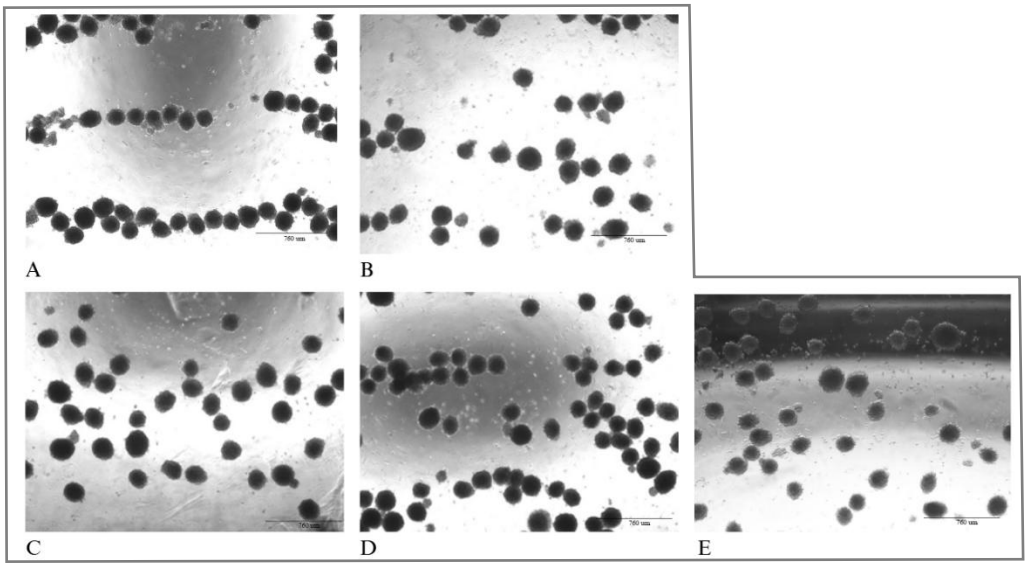

Figure 3.31 - 4x EVOS images of spheroids captured 2 min after acoustics were turned on with 50 V. A - 4-Well with Agarose; B - 4-Well with Anti-Adherence solution; C - 8-Well with Agarose; D – 8-Well with Anti-Adherence solution; E – 8-Well from previous experiment (Section 3.3.8).

Agarose in the 4-Well (Figure 3.31A) was the configuration that allowed the most organized alignment, with spheroids aligned in visually clear bands. In both Figures 3.31B and 3.31D, it is possible to observe some bands of spheroids, despite their distortion. Agarose in the 8-Well (Figure 3.31C) did not promote any alignment and spheroids are randomly distributed, similar to not having any coat layer (Figure 3.31E). Based on these results, the dimensions of the chamber may play a more important role in promoting a better movement and alignment of spheroids than the presence of a bottom layer. Therefore, an additional analysis was conducted to determine which chamber size allowed a higher amplitude after propagation.

The amplitude inside a 4-Well Ibidi chamber was measured for different combinations of internal and external water volumes, and for an input voltage of 20 V. This chamber is approximately twice the size of an 8-Well, so the internal volumes considered were 240 – 600 µl, with steps of 20 µl. Figure 3.32 shows the measured amplitudes for each water volume.

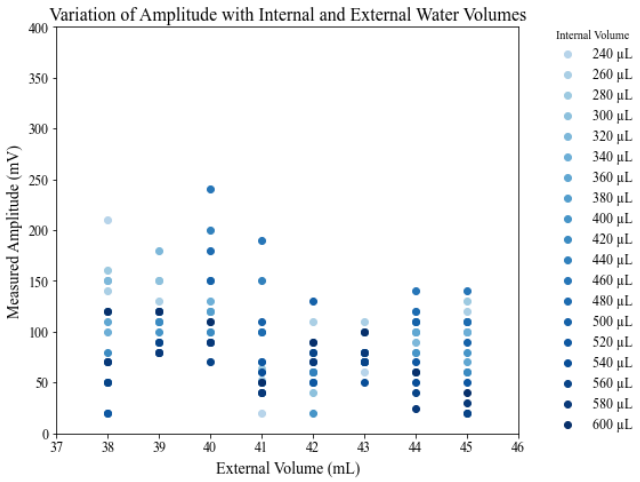

Figure 3.32 - Measured amplitude in a 4-Well Ibidi chamber for different water volumes.

The maximum registered amplitude was 240 mV (for an internal volume of 460 µl and an external volume of 40 ml). This amplitude is greater than the maximum registered in a chamber of an 8-Well – 220 mV (section 3.3.7.). To confirm these results, both experiments were repeated (Figure 3.33 and Figure 3.34).

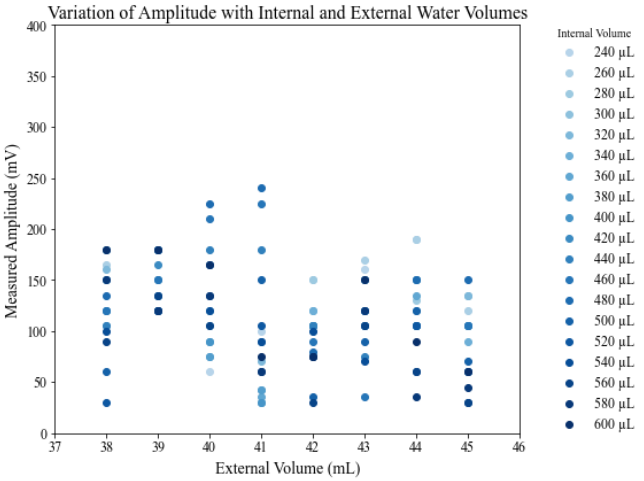

Figure 3.33 - Measured amplitude in a 4-Well Ibidi chamber for different water volumes.

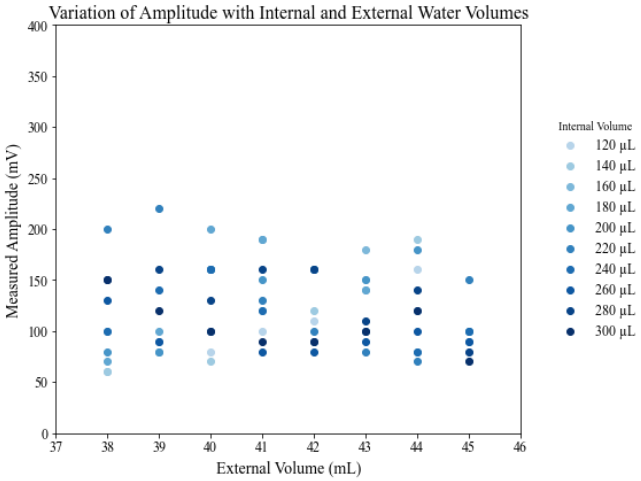

Figure 3.34 - Measured amplitude in an 8-Well Ibidi chamber for different water volumes.

The 4-Well exhibited the greatest measured amplitude (250 mV), while the 8-Well exhibited a maximum of 220 mV once again. To conclude with certainty that the 4-Well allows greater amplitudes than the 8-Well, more experiments are needed. Nevertheless, this is theoretically expected, since the 4-Well has fewer discontinuities the acoustic wave needs to go through.

The maximum amplitudes measured for both slides were obtained by different water volume combinations from those previously obtained. The origin of these variations may be the distribution of water, which is most likely different from experiment to experiment, and very difficult to control.

The amplitude inside Concept 3 was also measured for an input voltage of 20 V. In this setup, there are no chamber slides and there is only one type of volume to have in consideration. Thus, the water volume inside it was varied between 1.0 and 2.0 ml, with steps of 0.1 ml. This experiment was conducted twice, and the results are presented in Figure 3.35.

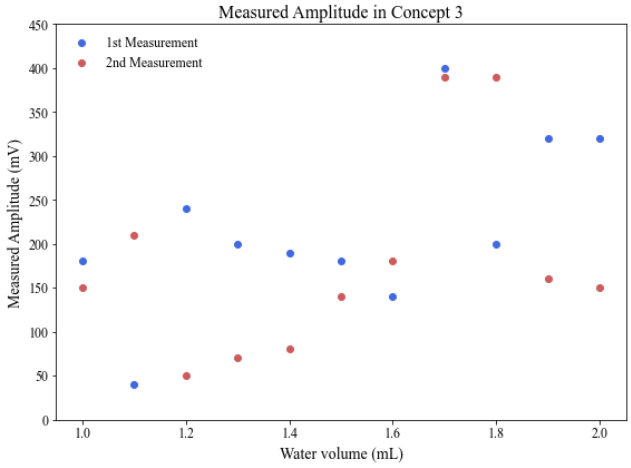

Figure 3.35 - Measured amplitudes in Concept 3 for different water volumes.

The maximum amplitude measured in this setup was 400 mV, which is greater than the amplitudes measured inside the 8- and 4-Well. These findings support the idea that chamber slides weaken the acoustic field and that setups such as Concept 3 allow a stronger ARF. Spheroid alignment was observed in this setup (Figure 3.29). However, this design needs to be optimized to minimize vibrations and modified to become sterilizable, so it could be used in further experiments. This was not possible to accomplish during this project, but it should be considered in future work.

Given these results, Setup B with a 4-Well slide coated with Agarose was considered the best option amongst all alternatives. Therefore, a design of experiments was conducted with this setup to understand the effects of different inputs on its performance.

3.4.3. Design of Experiments

In this phase, mean displacement and mean speed of the spheroids were determined and studied for different inputs of voltage and external water volumes. Spheroids were prepared and 460 µl of spheroid suspension was inserted into a middle chamber of a 4-Well slide, previously coated with an agarose layer. The slide was placed into Setup B and images were taken on the EVOS every 5 seconds, as soon as the experiments started. Two input voltages were tested: 20 and 30 V, and the water volume outside the chamber was varied between 38 and 45 ml. The input frequency was 0.992 MHz.

Initially, Setup B was filled with 38 ml of water and two experiments were conducted, one for each input voltage. Only then was the volume of water increased by 1 ml. This guaranteed the same exact water level between experiments, avoiding differences caused by measuring errors.

The results are presented in Figure 3.36.

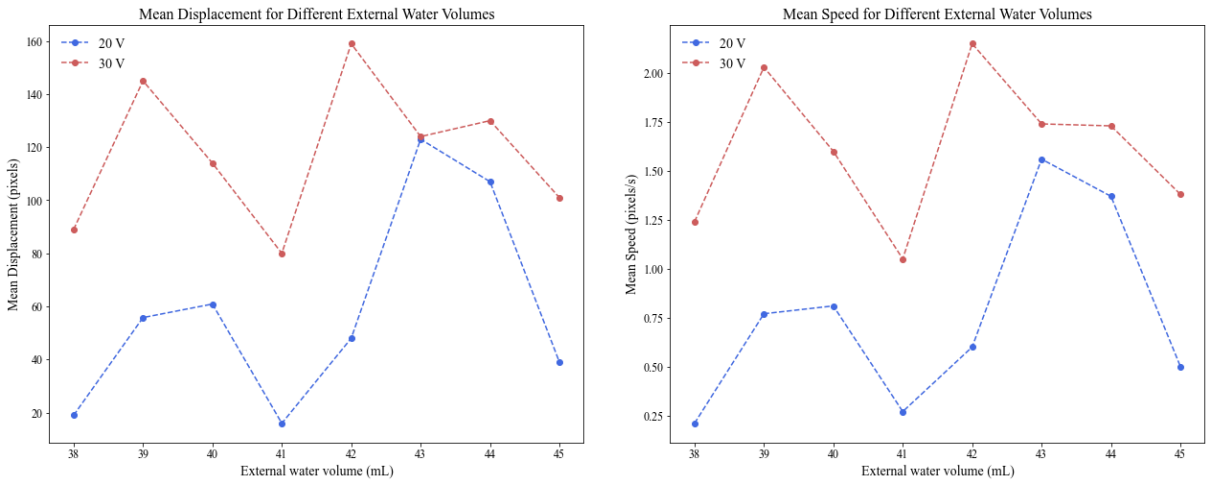

Figure 3.36 - Mean displacement (left) and mean average speed (right) for different external water volumes for two input voltages (20 V and 30 V).

These results show similar behaviour between mean displacement and speed, which exhibit similar trends when varying the water volume and the input voltage. Small differences in slopes are explained by the fact that the average speed takes into consideration the full path length of the spheroid and not only its net displacement.

As expected, both responses are greater for an input voltage of 30 V than for 20 V. However, it is noticeable that the movement of the spheroids is not proportional to this parameter, as their behaviour is different. These differences between the blue and the orange graphs might be explained by several factors. The distribution of the spheroids in the chamber is never the same between experiments, and single spheroids move more easily than clustered spheroids, which have forces acting between them. Also, although the region of the chamber to capture images was meant to be the same for all experiments, when not enough spheroids were in it, a different region was selected. Additionally, higher voltages are associated with stronger acoustic streaming, which impacts spheroid movement.

For an input of 20 V, spheroids moved towards the nodes, but they accumulated and grouped together, and bands were not created (Figure 3.37A). For 30 V, this grouping was less evident, although the alignment was still poorly defined, as shown by Figure 3.37B.

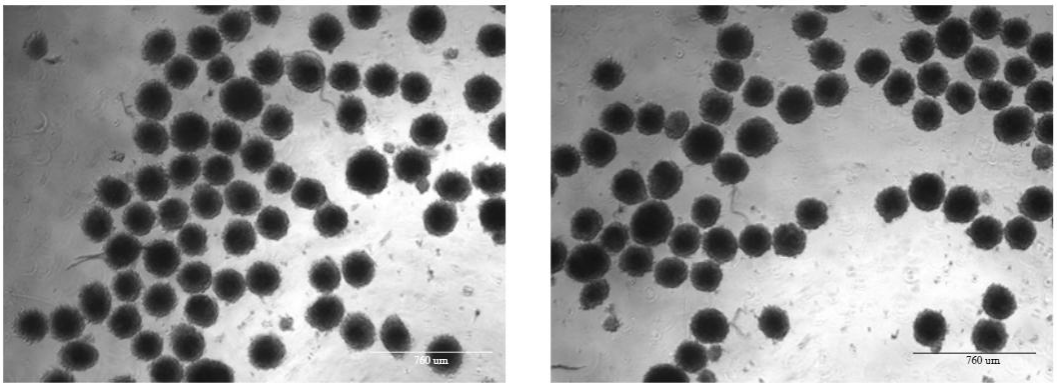

A B

Figure 3.37 - 4x EVOS images of spheroids in a 4-Well Ibidi chamber with Agarose. A - Input voltage of 20 V and B - Input voltage of 30 V.

It would be interesting to extend these experiments for input voltages of 40 V and 50 V, since they are expected to increase spheroid displacement and create a more defined and less distorted alignment.

This DOE consisted in the last experiments conducted within this dissertation. It showed the impact of two different factors in spheroid movement, enhancing the potential of having an agarose coat on a wide chamber as a strategy to reduce adhesion forces and promote a more defined alignment.

Chapter 4

Conclusion

The work developed in this dissertation allowed for exploring the potential of acoustic manipulation for tissue engineering, particularly in promoting the alignment of HDF spheroids. By applying the DMADV methodology from Six-Sigma, it was possible to identify the problems of current setups that researchers wanted to solve and their requirements for a new alternative. Measurement systems were established for each requirement, and an experimental analysis was performed to understand and optimize factors that influence the acoustic field and spheroid movement.

The results demonstrated that the chosen frequency influences the energy loss and that 0.992 MHz is the optimized value for the PIC181 transducers. It was also demonstrated that the propagation material impact the alignment time of particles, revealing that water is more appropriate than ultrasound gel. Amplitude measurements showed differences between current setups and highlighted the impact of changing the distance between the transducers. The analysis performed on Setup B to understand the influence of different water volumes inside and outside the slide chamber demonstrated the variation caused by these parameters on the amplitude of the wave. The script developed in Python enabled the identification of volume ranges that enhance the strength of the acoustic field. Tests with spheroids confirmed the impact of input voltage, frequency and water volumes on the acoustic field and consequently on their displacement.

The analysis performed during this project allowed the development of a QFD, first and second matrices, where customer requirements were converted into CTQs and CTQs were translated into product features. From this, concept designs were developed and assessed by their potential. Other parameters, such as chamber size and surface treatments, were considered in these concepts. The Design phase focused on prototyping and running pilot tests, which showed that placing spheroids on a 4-Well pre-treated with Agarose is a promising strategy to enhance their displacement and alignment.

Overall, the work developed during this dissertation allowed a better understanding of how different factors can influence acoustic wave transmission and spheroid alignment. By systematically exploring these factors and developing experimental tools and prototypes, this research provides valuable insights for future advancements in the field of acoustic manipulation in tissue engineering.

4.1. Limitations and Future Work

Throughout this study, different limitations of the adopted methods were found. First, on experiments with both particles and spheroids, there was a need to disrupt their alignment between tests. In order to guarantee that, before turning on the acoustic equipment, they were well distributed in the chamber. This was performed by slightly shaking the slide, which is not a consistent method, and the results depend on factors such as the strength of the movement. Additionally, when the aim was to analyse the alignment and/or the displacement of particles or spheroids, the images were captured on regions that seemed to produce good results on preliminary tests. However, in some cases, due to

particles and spheroids' heterogeneous distribution across the chamber, those regions did not yield representative results. In those occasions, experiments were repeated in different regions where a number of particles or spheroids was considered to be sufficient to represent their overall behaviour. This was considered a limitation, since comparisons between experiments were established for different areas of the chamber, which have different acoustic pressures. Therefore, other alternatives for this method should be considered in future experiments.

Time to align was assessed using a Voronoï Tessellation, created by an ImageJ script. This approach was previously used by Armstrong et al. [24], who demonstrated the effectiveness of this method in obtaining important quantitative values for cell patterning assessment. However, the script developed in this dissertation is different from the one developed by Armstrong et al. [24]. During microparticle analysis, it was noticed that, for some images, the script failed to detect all particles. Hence, enhancements of this method are needed to optimize detection accuracy and consequently improve the reliability of alignment assessment.

Spheroid analyses relied on mean displacement and mean average speed, which represent indirect measures of the ARF but do not quantify or qualify alignment. The alignment was only assessed by visual inspection, a subjective and biased method.

The work developed throughout this dissertation provided valuable insights, even though the specific parameter values for an optimized setup were not fully determined. Prototypes were developed and pilot runs were conducted, which highlighted the influence of factors such as water volume on experimental variability. These observations revealed important limitations in the methods, indicating areas where further control and refinement are needed. Future work should aim to identify and minimize sources of variability, for which modelling software, such as COMSOL Multiphysics, could be particularly useful in studying the pressure fields and informing optimization of the setup. Additionally, Design Concepts 1 and 2, which were neither printed nor tested, should be considered in future experiments as potential alternatives to Setup B.

References

[1] - Saidi, R. F., Kenari, S. K. H., & Saidi, R. F. (n.d.). Challenges of Organ Shortage for Transplantation: Solutions and Opportunities. In *International Journal of Organ Transplantation Medicine*. www.ijotm.com

[2] - Parveenns, & Krishnakumarrk. (2006). *ReviewArticle NewErainHealthCare:TissueEngineering* (Vol. 1, Issue 1). www.pubstemcell.com

[3] - Lombello, C.B., Masson, A.O., Ambrosio, F.N., Ferraraz, D.C., do Nascimento, M.H.M. (2023). Principles of Tissue Engineering and Regenerative Medicine. In *Lombello, C.B., da Ana, P.A. (eds) Current Trends in Biomedical Engineering*. Springer, Cham. https://doi.org/10.1007/978-3-031-38743-2_8

[4] - Lynch, C. R., Kondiah, P. P. D., & Choonara, Y. E. (2021). Advanced strategies for tissue engineering in regenerative medicine: A biofabrication and biopolymer perspective. *Molecules*, *26*(9). https://doi.org/10.3390/molecules26092518

[5] - Howard, D., Buttery, L. D., Shakesheff, K. M., & Roberts, S. J. (2008). Tissue engineering: Strategies, stem cells and scaffolds. In *Journal of Anatomy* (Vol. 213, Issue 1, pp. 66–72). https://doi.org/10.1111/j.1469-7580.2008.00878.x

[6] - Smith, A. S. T., Yoo, H., Yi, H., Ahn, E. H., Lee, J. H., Shao, G., Nagornyak, E., Laflamme, M. A., Murry, C. E., & Kim, D. H. (2017). Micro-and nano-patterned conductive graphene-PEG hybrid scaffolds for cardiac tissue engineering. *Chemical Communications*, *53*(53), 7412–7415. https://doi.org/10.1039/c7cc01988b

[7] - Chae, S. J., Hong, J., Hwangbo, H., & Kim, G. H. (2021). The utility of biomedical scaffolds laden with spheroids in various tissue engineering applications. *Theranostics*, *11*(14), 6818–6832. https://doi.org/10.7150/thno.58421

[8] - Vuille-Dit-Bille, E., Deshmukh, D. V., Connolly, S., Heub, S., Boder-Pasche, S., Dual, J., Tibbitt, M. W., & Weder, G. (2022). Tools for manipulation and positioning of microtissues. In *Lab on a Chip* (Vol. 22, Issue 21, pp. 4043–4066). Royal Society of Chemistry. https://doi.org/10.1039/d2lc00559j

[9] - Lu, K., Qian, Y., Gong, J., Zhu, Z., Yin, J., Ma, L., Yu, M., & Wang, H. (2021). Biofabrication of aligned structures that guide cell orientation and applications in tissue engineering. In *Bio-Design and Manufacturing* (Vol. 4, Issue 2, pp. 258–277). Springer. https://doi.org/10.1007/s42242-020-00104-5

[10] - Ahrens, J. H., Uzel, S. G. M., Skylar-Scott, M., Mata, M. M., Lu, A., Kroll, K. T., & Lewis, J. A. (2022). Programming Cellular Alignment in Engineered Cardiac Tissue via Bioprinting Anisotropic Organ Building Blocks. *Advanced Materials*, *34*(26). https://doi.org/10.1002/adma.202200217

[11] - Armstrong, J. P. K., Puetzer, J. L., Serio, A., Guex, A. G., Kapnisi, M., Breant, A., Zong, Y., Assal, V., Skaalure, S. C., King, O., Murty, T., Meinert, C., Franklin, A. C., Bassindale, P. G., Nichols, M. K., Terracciano, C. M., Hutmacher, D. W., Drinkwater, B. W., Klein, T. J., … Stevens, M. M. (2018). Engineering Anisotropic Muscle Tissue using Acoustic Cell Patterning. *Advanced Materials*, *30*(43). https://doi.org/10.1002/adma.201802649

[12] - Guex, A. G., Di Marzio, N., Eglin, D., Alini, M., & Serra, T. (2021). The waves that make the pattern: a review on acoustic manipulation in biomedical research. In *Materials Today Bio* (Vol. 10). Elsevier B.V. https://doi.org/10.1016/j.mtbio.2021.100110

[13] - Kang, B., Shin, J., Park, H. J., Rhyou, C., Kang, D., Lee, S. J., Yoon, Y. sup, Cho, S. W., & Lee, H. (2018). High-resolution acoustophoretic 3D cell patterning to construct functional collateral cylindroids for ischemia therapy. *Nature Communications*, *9*(1). https://doi.org/10.1038/s41467-018-07823-5

[14] - Guo, F., Mao, Z., Chen, Y., Xie, Z., Lata, J. P., Li, P., Ren, L., Liu, J., Yang, J., Dao, M., Suresh, S., & Huang, T. J. (2016). Three-dimensional manipulation of single cells using surface acoustic waves. *Proceedings of the National Academy of Sciences of the United States of America*, *113*(6), 1522–1527. https://doi.org/10.1073/pnas.1524813113

[15] - Sahin, M. A., Ali, M., Park, J., & Destgeer, G. (2024). *Fundamentals of Acoustic Wave Generation and Propagation*.

[16] - Saheban, H., & Kordrostami, Z. (2021). Hydrophones, fundamental features, design considerations, and various structures: A review. In *Sensors and Actuators, A: Physical* (Vol. 329). Elsevier B.V. https://doi.org/10.1016/j.sna.2021.112790

[17] - Yucel-Finn, A., McKiddie, F., Prescott, S., & Griffiths, R. (2023). Imaging with ultrasound. In *Farr's Physics for Medical Imaging* (3rd ed.). Elsevier.

[18] - Liu, Y., Yin, Q., Luo, Y., Huang, Z., Cheng, Q., Zhang, W., Zhou, B., Zhou, Y., & Ma, Z. (2023). Manipulation with sound and vibration: A review on the micromanipulation system based on sub-MHz acoustic waves. In *Ultrasonics Sonochemistry* (Vol. 96). Elsevier B.V. https://doi.org/10.1016/j.ultsonch.2023.106441

[19] - Science Ready. (n.d.). *Standing waves in pipes: Everything explained – HSC physics*. Science Ready.https://scienceready.com.au/pages/standing-wave-in-pipes?srsltid=AfmBOoq9UO-YNXPgPqG0wjM7gVR-3ukUqqFqKK8dXMIAemv-RcPsibfC#google_vignette

[20] - Pazos Ospina, J. F., Contreras, V., Estrada-Morales, J., Baresch, D., Ealo, J. L., & Volke-Sepúlveda, K. (2022). Particle-Size Effect in Airborne Standing-Wave Acoustic Levitation: Trapping Particles at Pressure Antinodes. *Physical Review Applied*, *18*(3). https://doi.org/10.1103/PhysRevApplied.18.034026

[21] - Hill, M., & Harris, N. R. (2007). Ultrasonic particle manipulation. In *Microfluidic Technologies for Miniaturized Analysis Systems* (pp. 357–392). Springer US. https://doi.org/10.1007/978-0-387-68424-6_9

[22] - Pérez, N., Andrade, M. A. B., Canetti, R., & Adamowski, J. C. (2014). Experimental determination of the dynamics of an acoustically levitated sphere. *Journal of Applied Physics*, *116*(18). https://doi.org/10.1063/1.4901579

[23] - Shi, J., Ahmed, D., Mao, X., Lin, S. C. S., Lawit, A., & Huang, T. J. (2009). Acoustic tweezers: Patterning cells and microparticles using standing surface acoustic waves (SSAW). *Lab on a Chip*, *9*(20), 2890–2895. https://doi.org/10.1039/b910595f

[24] - Armstrong, J. P. K., Maynard, S. A., Pence, I. J., Franklin, A. C., Drinkwater, B. W., & Stevens, M. M. (2019). Spatiotemporal quantification of acoustic cell patterning using Voronoï tessellation. *Lab on a Chip*, *19*(4), 562–573. https://doi.org/10.1039/c8lc01108g

[25] - Zheng, X., Apfel, R. E. (1995) Acoustic interaction forces between two fluid spheres in an acoustic field. J. *Acoust. Soc. Am* 97, 2218–2226.

[26] - Saeidi, D., Saghafian, M., Javanmard, S. H., & Wiklund, M. (2020). A quantitative study of the secondary acoustic radiation force on biological cells during acoustophoresis. *Micromachines*, *11*(2). https://doi.org/10.3390/mi11020152

[27] - Bhargava, N., Mor, R. S., Kumar, K., & Sharanagat, V. S. (2021). Advances in application of ultrasound in food processing: A review. In *Ultrasonics Sonochemistry* (Vol. 70). Elsevier B.V. https://doi.org/10.1016/j.ultsonch.2020.105293

[28] - Butt, Z., Anjum, Z., Sultan, A., Qayyum, F., Khurram Ali, H. M., & Mehmood, S. (2017). Investigation of electrical properties & mechanical quality factor of piezoelectric material (PZT-4A). *Journal of Electrical Engineering and Technology*, *12*(2), 846–851. https://doi.org/10.5370/JEET.2017.12.2.846

[29] - Fan, Y., Wang, X., Ren, J., Lin, F., & Wu, J. (2022). Recent advances in acoustofluidic separation technology in biology. In *Microsystems and Nanoengineering* (Vol. 8, Issue 1). Springer Nature. https://doi.org/10.1038/s41378-022-00435-6

[30] - Scholz, M. S., Drinkwater, B. W., Llewellyn-Jones, T. M., & Trask, R. S. (2015). Counterpropagating wave acoustic particle manipulation device for the effective manufacture of composite materials. *IEEE Transactions on Ultrasonics, Ferroelectrics, and Frequency Control*, *62*(10), 1845–1855. https://doi.org/10.1109/TUFFC.2015.007116

[31] - Chen, B., Wu, Z., Wu, Y., Chen, Y., & Zheng, L. (2023). Controllable fusion of multicellular spheroids using acoustofluidics. *Microfluidics and Nanofluidics*, *27*(7). https://doi.org/10.1007/s10404-023-02660-5

[32] - Meng, Y., Zhang, J., Hong, Z., & Drinkwater, B. W. (2025). Numerical and experimental study of circular array to enhance acoustic tweezer-based particle manipulation. *Ultrasonics*, *152*. https://doi.org/10.1016/j.ultras.2025.107647

[33] - Courtney, C. R. P., Ong, C. K., Drinkwater, B. W., Bernassau, A. L., Wilcox, P. D., & Cumming, D. R. S. (2012). Manipulation of particles in two dimensions using phase controllable ultrasonic standing waves. *Proceedings of the Royal Society A: Mathematical, Physical and Engineering Sciences*, *468*(2138), 337–360. https://doi.org/10.1098/rspa.2011.0269

[34] - Costa, E. C., de Melo-Diogo, D., Moreira, A. F., Carvalho, M. P., & Correia, I. J. (2018). Spheroids Formation on Non-Adhesive Surfaces by Liquid Overlay Technique: Considerations and Practical Approaches. *Biotechnology journal*, *13*(1), 10.1002/biot.201700417. https://doi.org/10.1002/biot.201700417

[35] - *STEMCELL Technologies*. Available at: https://www.stemcell.com/products/aggrewell-rinsing-solution.html#section-resources-and-publications

[36] - Pyzdek, Thomas. (2003). *The Six Sigma handbook : a complete guide for green belts, black belts, and managers at all levels*. McGraw-Hill.

Appendices

1. Appendix A

Figure A1 shows the behaviour of microparticles under an acoustic field of 22 V for different frequencies (see Section 3.3.1).

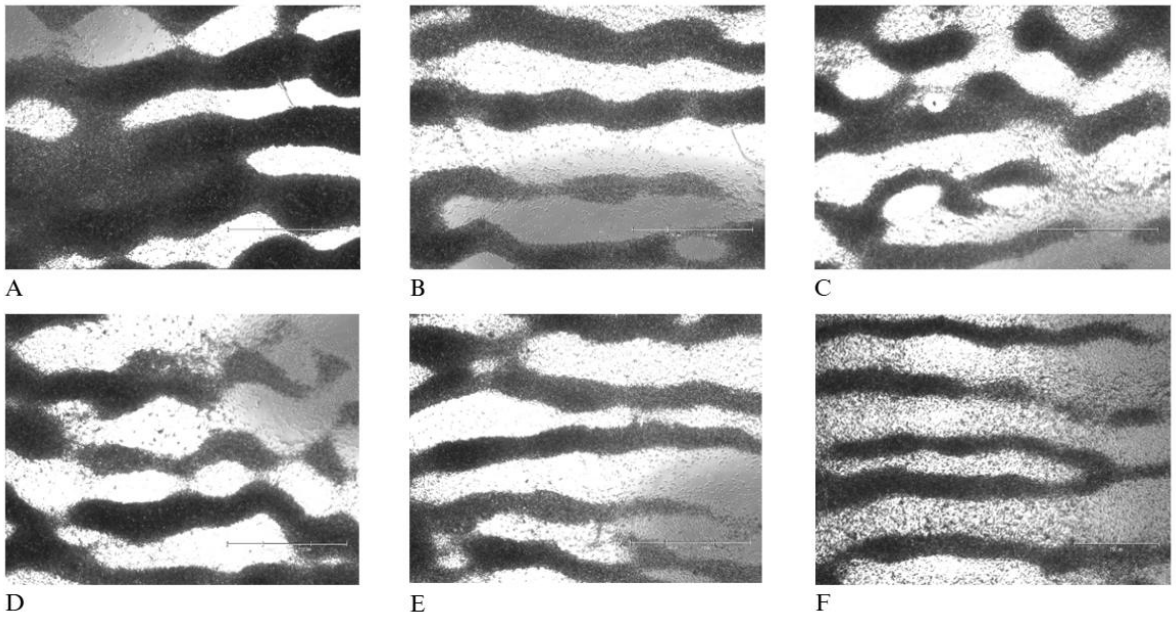

Figure A1 - 4x EVOS images of microparticles under an acoustic field of 22 V. A - 0.96 MHz; B - 0.98 MHz; C - 0.99 MHz; D - 1.16 MHz; E - 1.18 MHz; F - 1.19 MHz.

2. Appendix B

Table B1 shows the results of the 16 experiments conducted in 3.3.1 with microparticles, for different combinations of factors. The Voronoï areas detected in six of these experiments, highlighted in grey, did not change over time. In these cases, time to align and wave distortion were not determined and were considered as the worst result.

Table B1 - Time to align and wave distortion normalized for each experiment with microparticles.

Experiment	**Factors**				**Responses**	
	Voltage (V)	Acoustic refractive index (relative to water)	Volume of particles (µl)	Frequency (MHz)	Time to align normalized (1 – No alignment; 0 – Minimum time to align)	Wave distortion normalized (1 – No alignment; 0 – No distortion)
1	18	0.938	2.0	1.0	1.0	1.0
2	30	0.938	2.0	1.0	0.56	0.74
3	18	1.0	2.0	1.0	0.59	0.47
4	30	1.0	2.0	1.0	0.27	0.59
5	18	0.938	5.0	1.0	1.0	1.0
6	30	0.938	5.0	1.0	0.78	0.45
7	18	1.0	5.0	1.0	0.22	0.45
8	30	1.0	5.0	1.0	0.32	0.59
9	18	0.938	2.0	1.15	1.0	1.0
10	30	0.938	2.0	1.15	0.73	0.61
11	18	1.0	2.0	1.15	0.68	0.37
12	30	1.0	2.0	1.15	0.42	0.79
13	18	0.938	5.0	1.15	1.0	1.0
14	30	0.938	5.0	1.15	1.0	1.0
15	18	1.0	5.0	1.15	1.0	1.0
16	30	1.0	5.0	1.15	0.39	0.33

3. Appendix C

Table C1 shows the results of the Sample *t*-tests performed in section 3.3.2.

Table C1 - Results of the Sample t-tests performed in 3.3.2 to understand the minimum number of replicates per setup required to detect the observed mean difference with 80% power ($\alpha = 0.05$).

Pair	Frequency (MHz)	Setup #1	Setup #2	Voltage (V)	Mean Difference in amplitude	Pooled Standard Deviation	Sample Size per Group
1	1.00	Setup B	Setup C	10	0.0456	0.0493	20
2	1.00	Setup B	Setup C	20	0.0499	0.0453	14
3	1.00	Setup B	Setup C	30	0.0546	0.0519	16
4	1.00	Setup B	Setup D	10	0.0327	0.0511	40
5	1.00	Setup B	Setup D	20	0.0336	0.0483	34
6	1.00	Setup B	Setup D	30	0.0413	0.0539	28
7	1.00	Setup C	Setup D	10	0.0129	0.0428	175
8	1.00	Setup C	Setup D	20	0.0163	0.0394	94
9	1.00	Setup C	Setup D	30	0.0133	0.0421	159
10	1.15	Setup B	Setup C	10	0.0234	0.0261	21
11	1.15	Setup B	Setup C	20	0.0237	0.0243	18
12	1.15	Setup B	Setup C	30	0.0254	0.0259	18
13	1.15	Setup B	Setup D	10	0.0140	0.0275	62
14	1.15	Setup B	Setup D	20	0.0140	0.0254	53
15	1.15	Setup B	Setup D	30	0.0151	0.0281	56
16	1.15	Setup C	Setup D	10	0.0094	0.0215	83
17	1.15	Setup C	Setup D	20	0.0097	0.0204	70
18	1.15	Setup C	Setup D	30	0.0103	0.0219	73